Michael Vorderderfler, BSc

Design of a miniaturized dual-band RFID antenna for an eWLB package

Master's Thesis

Submitted as thesis to attain the academic degree

Master of Science

Telematics

at the

Graz University of Technology

Supervisor
Dipl.-Ing. Dr.techn. Michael Gadringer
Institute for Microwave and Photonic Engineering (IHF)

Infineon Technologies Austria AG

Graz, June 2016

This master thesis has been supported by
Infineon Technologies Austria AG

Declaration of Authorship

I declare that I have authored this thesis independently, that I have not used other than the declared sources/resources, and I have explicitly indicated all material which has been quoted either literally or by content from the sources used. The text document uploaded to TUGRAZonline is identical to the present master's thesis dissertation.

Date

Signature

Zusammenfassung

In der heutigen Zeit ist die Vernetzung von elektronischen Geräten ein immer größeres Thema. Die Automatisierung von Vorgängen im industriellen wie auch im privaten Bereich wird immer häufiger eingesetzt. Drahtlose wie auch kabelgebundene Netzwerke sind entscheidend für die Realisierung dieser Automatisierungsaufgaben. Der Nachteil von kabelgebundenen Netzwerken ist die gerine Flexibilität bei Änderungen an bestehenden Systemen. Drahtlose Netzwerke lassen sich flexibel aufbauen bzw. erweitern. Diese Arbeit bezieht sich auf drahtlose *Home Automation* Systeme. Die Erfordernisse für den reibungslosen Betrieb eines solchen Systems, liegen zum einen in hoher Effizienz der einzelnen Elemente und hohen Sicherheitsanforderungen bezüglich der Kommunikation zwischen den Elementen. Um diese Bedingungen zu erfüllen, benötigen alle Komponenten zumindest zwei Kommunikationsinterfaces. Diese Arbeit beschreibt die Entwicklung eines drahtlosen Sensorknotens mit diesen beiden Interfaces, wobei diese bei zwei unterschiedlichen Frequenzen realisiert wurden.

Dieses Projekt wurde in Zusammenarbeit mit der Infineon Technologies Austria AG und dem Institut fuer Hochfrequenztechnik der Technischen Universitaet Graz im Rahmen des Projekts SeCoS (Secure Contactless Sphere) durchgeführt. Die benötigten Ressourcen wurden dabei von der Firma Infineon Technologies Austria AG bereitgestellt.

Im Zuge des Projekts wurden zwei verschiedene Implementierungen für den Sensorknoten erarbeitet. Eine stark miniaturisierte Variante als System-In-Package Ausführung und eine Implementierung auf Leiterplatten Technologie. Ein von Infineon Technologies Austria AG entwickelten Chip, welcher als Controller agiert und ein drahtloses Interface im HF-Frequenzbereich zur Verfügung stellt. Ein ebenso von Infineon Technologies Austria AG entwickelter Transceiver für UHF Frequenzen bietet weitere Kommunikationsmöglichkeiten. Für dieses System wurden unterschiedliche Antennentypen entwickelt, simuliert, produziert und charakterisiert.

Die größte Herausforderung zeigte sich in der durch die Miniaturisierung stark verringerten Antennenfläche, was sich auf die Leistung der Antennen auswirkt.

Diese Masterarbeit gliedert sich in einen Theorieteil welcher Grundlagen zu Hochfrequenztechnik und Antennen erläutert, weiters einer Systembeschreibung des zu implementierenden Sensorknotens, die Entwicklung und Simulation der Antennen, die Implementierung des gesamten Systems und einer Charakterisierung der produzierten Antennen. Abschließend werden noch Möglichkeiten zur Weiterentwicklung und eine rückblickende Zusammenfassung aufgeführt.

Abstract

Industrial machine-to-machine communications, internet of things and home automation systems gain more and more importance. Especially in home automation, a flexible network is advantageous to cope with charging requirements. On the one hand wireless networks are able to provide this flexibility. On the other hand special care has to be taken to secure the wireless communication.

In this thesis, the focus is put onto wireless home automation systems. Such systems have high efficiency, and at the same time, high security requirements. For this purpose, a wireless dual band sensor node was designed, including UHF and HF interfaces. The primary focus of present work lies on the antenna design and characterization.

The whole project was accomplished in a cooperation between Infineon Technologies Austria AG and the Institute of Microwave and Photonic Engineering, Graz University of Technology. Most of the practical work was performed at Infineon Technologies Austria AG and the analyze of the implementation was done at the Graz University of Technology.

In order to meet the high integration requirements of sensor applications, two different approaches to system design were investigated: high miniaturized system in package and printed circuit board implementation. A microchip, developed by Infineon Technologies Austria AG, acts as controller and provides the HF interface. An additional transceiver, also developed by Infineon Technologies Austria AG, provides the UHF interface of the sensor node. For these interfaces, different antennas were designed, simulated, manufactured and evaluated.

The mentioned implementations presented a number of challenges. High miniaturization significantly decreases antenna performance: a trade-off between size and efficiency of the system had to be derived.

This thesis includes a general introduction into the theory of high frequency applications and antennas, the description of the used packaging technology, an overview of the whole system of the sensor node, the design and simulation of the antennas, the implementation of the sensor node and characterizations of the developed antennas.

Acknowledgement

First I would like to express my gratitude to Dipl-Ing. Dr.techn. Michael Ernst Gadringer from the Institute of Microwave and Photonic Engineering at the Graz University of Technology for his patient guidance and support along the challenging way to this thesis.

Furthermore I would like to thank to Dipl.-Ing. Gerald Holweg, head of the Contactless and Radio Frequency Exploration (CRE) department of Infineon Technolgies Austria AG, for making this thesis happen in cooperation with an innovative industrial partner, such as Infineon Technologies Austria AG.

I would also like to thank my colleagues at the CRE department for their technical and personal advise and the enjoyable working atmosphere.

A big thank you also goes to my parents Christine and Johann for motivating me and always providing backup during my study.

Graz, June 2016 Michael Vorderderfler

Contents

1 Introduction **1**

2 Theory **5**

2.1 Circuit Theory 5

2.2 Antenna Parameters 14

2.3 Antenna Types 20

2.3.1 Wire Antennas 20

2.3.2 Patch Antennas 21

2.4 The Smith Chart 24

3 Embedded Wafer-Level Ball Grid Array **27**

3.1 Internal Structure and Process Flow of eWLB 29

3.2 Design Restrictions 30

4 System Overview **31**

4.1 System Description 31

4.2 Onboard communication 33

4.3 HF Interface 34

4.4 UHF Interface 34

5 Antenna Design and Simulations **36**

5.1 eWLB Antenna Design 36

5.1.1 Inverted F Antenna 37

5.1.2 Loop Antenna 42

5.2 Design for direct Integration on a Printed Circuit Board 45

5.2.1 Inverted F Antenna 47

5.2.2 Loop Antenna 53

5.2.3 Monopole Antenna 56

5.2.4 HF Antenna 60

6 System Design - Implementation **63**

6.1 Circuit Design 63

6.2 PCB for Chip-on-Board Design 64

6.3 Firmware 67

7 Antenna Measurements **70**

7.1 Inverted F Antennas 71

7.2 Loop Antenna 76

7.3 Monopole Antenna 77

8 Conclusion and Outlook **79**

Appendix A Schematics and Layout documents **81**

List of Figures

1.1 Overview of a home automation system connected to a small selection of sensors (red) and a control unit (blue) . . . 1
1.2 Establishing secure communication by firstly exchanging keys (a), and using them to encrypt the data transfer between wireless device and control station (b) . . . 3

2.1 Simple schematic with generator and load . . . 5
2.2 Simple circuit where generator and load are connected through a transmission line . . . 6
2.3 Transmission line model of a homogeneous line in z-direction . . . 7
2.4 Input resistance $Z_{IN}(z)$ and reflection coefficients Γ at entrance and end of the transmission line . . . 9
2.5 Voltage distribution on a line at different values $\Gamma = 1$ and $\Gamma > 0$ . . . 10
2.6 Structure of a microstrip line . . . 12
2.7 Directivity characteristics of an isotropic and directive antenna in a two dimensional view . . . 15
2.8 Near and Far field regions of an antenna . . . 17
2.9 Fields of an oscillating charge dipole for different instants of time [1] . . . 18
2.10 Reactive elements of a dipole antenna . . . 19
2.11 Current distribution on a dipole antenna for different dipole length l . . . 20
2.12 Monopole antenna over a perfect ground plane (a), and the equivalent dipole in free space (b) . . . 21
2.13 Patch antenna with feed line (a), and a cross section of the antenna showing the electric field (b) . . . 22
2.14 Schematic structure of a printed Inverted F antenna. The capacitor C and inductance L represent the equivalent elements of a transmission line model 23
2.15 Schematic structure of the printed loop antenna (a) and the equivalent circuit (b) . . . 23
2.16 The Smith Chart . . . 24
2.17 Graphical representation of the reflection coefficient in the smith chart . . . 25
2.18 Impedance representation on the Smith Chart . . . 26

3.1 Interconnection gap between package and printed circuit board [2] . . . 29

3.2 Production process of eWLB [3] 30

4.1 Block diagram of the whole wireless sensor node 31
4.2 Near field magnetic coupling of two wireless devices 34
4.3 UHF protocol; 2kbit FSK EU pattern 35

5.1 Partition of the eWLB 36
5.2 Substrate model of the eWLB package 37
5.3 Design of inverted F antenna for the eWLB 38
5.4 Simulated S11 parameter of the inverted F antenna for the eWLB 39
5.5 Smith chart for the inverted F antenna for the eWLB 40
5.6 Simulation results of the antenna gain and efficiency of the eWLB inverted F antenna at different conditions 41
5.7 Design of the loop antenna for the eWLB 42
5.8 Simulated S11 parameter of the loop antenna for the eWLB 43
5.9 Smith chart for the loop antenna for the eWLB 44
5.10 Simulation results of the antenna gain and efficiency of the eWLB loop antenna at different conditions 45
5.11 Partition of the printed circuit board 46
5.12 Substrate model of the printed circuit board 46
5.13 Design of inverted F antenna v1 47
5.14 Design of inverted F antenna v2 48
5.15 Current distribution of the Inverted F antenna type 1 49
5.16 Current distribution of the Inverted F antenna type 2 49
5.17 Simulated S11 parameter of both inverted F antennas 50
5.18 Smith diagram of both inverted F antennas 51
5.19 Simulation results of the antenna gain and efficiency of IFAv1 at different conditions 52
5.20 Simulation results of the antenna gain and efficiency of IFAv2 at different conditions 52
5.21 Design of the loop antenna 53
5.22 Current distribution of the loop antenna 54
5.23 Simulation of S11 parameter of the loop antenna 54
5.24 Smith diagram of the loop antenna 55
5.25 Simulation results of the antenna gain and efficiency of the Loop antenna at different conditions 56
5.26 Design of monopole antenna 57
5.27 Current distribution of the monopole antenna 57
5.28 Monople S11 parameter with (blue) and without (red) loading coil 58
5.29 Smith diagram of the monopole antenna 59

5.30 Simulation results of the antenna gain and efficiency of the Monopole antenna at different conditions 60
5.31 Design of HF antenna 61
5.32 Simulation setup for the matching network of the HF antenna 61
5.33 Simulation results of the S11 simulation of the HF antenna for two different matching networks 62

6.1 Power supply of the wireless sensor node 63
6.2 Matching network and external circuitry of the UHF transceiver 64
6.3 Printed circuit board layout of the wireless sensor node 65
6.4 Detailed view of the matching network 65
6.5 The manufactured wireless sensor node on the PCB 66
6.6 Blockdiagram of the developed test firmware 67
6.7 Blockdiagram: configuration of the TDA5340 68
6.8 Blockdiagram: send test pattern 69

7.1 Measurement setup used for investigating the reflection coefficient of the different antennas 70
7.2 S11 simulation results of the IFAv1 antenna for different substrate permittivity 72
7.3 Simulation results of the IFAv1 antenna for different substrate permittivity plotted in the Smith Chart 72
7.4 Results of the reflection coefficient measurement of antenna IFAv1 with applied matching network 73
7.5 Smith diagram of antenna IFAv1 74
7.6 Results of the reflection coefficient measurement of antenna IFAv2 with applied matching network 75
7.7 Smith diagram of antenna IFAv2 75
7.8 Results of the reflection coefficient measurement of the loop antenna with applied matching network 76
7.9 Smith diagram of the loop antenna 77
7.10 Results of the reflection coefficient measurement of the monopole antenna with applied matching network 78
7.11 Smith diagram of the monopole antenna 78

A.1 Schematic of the wireless sensor node 82
A.2 Layout of the wireless sensor node 83
A.3 Layout of placement TOP side 83
A.4 Layout of placement BOTTOM side 84
A.5 TOP layer 84
A.6 Layout of metal layer TOP side with IFav1 84
A.7 Layout of metal layer BOTTOM side 85
A.8 Bonding plan for the ASIG controller 85

A.9 Bonding plan for the transceiver TDA5340 controller 86

List of Tables

5.1 Gain and efficiency of the eWLB inverted F antenna at 868 MHz; at different simulation conditions 41
5.2 Wavelength for FR4-PCB h=1.2 mm, $\epsilon_r = 4.6$, $\epsilon_{r,eff} = 3.2$ 47
5.3 Gain and Efficiency of both Inverted F antennas at 868 MHz; at different simulation conditions 53
5.4 Gain and efficiency of the loop antenna at 868 MHz; at different simulation conditions 56
5.5 Gain and Efficiency of the Monopole antenna at 868 MHz; at different simulation conditions 60

7.1 Measurement results for the inverted F antennas with and without additional matching at 868 MHz 73

List of Abbreviations

BGA	Ball Grid Array
dBm	Decibel-Milliwatts
eWBL	Embedded Wafer-Level Ball Grid Array
FIFO	First In, First Out
FSK	Frequency Shift Keying
IC	Integrated Circuit
IFA	Inverted F Antenna
IO	Input / Output
IRQ	Interrupt Request
MCP	Multi-Chip Package
MSB	Most Significant Bit
NFC	Near field communication
PCB	Printed Circuit Board
PIFA	Planar Inverted F Antenna
PoP	Stacked Package-on-Package
POR	Power-On Reset
RF	Radio Frequency
RFID	Radio Frequency identification
SFR	Special Function Registers
SiP	System in Package
SMT	Sub-Miniature-T
SoC	System on Chip
SPI	Serial Peripheral Interface
TML	Transmission Line
TSV	Through Silicon Vias
UHF	Ultra High Frequency
VNA	Vector Network Analyzer

Chapter 1

Introduction

In our world, nearly everything gets connected more and more, for example in the field of industrial applications, home automation or in the entertainment section. The requirements imposed on the interfaces providing the interconnectivity are often very high in terms of size or flexibility. Maximizing flexibility is often accomplished by using wireless instead of wired interfaces. This explains why wireless interfaces like Radio Frequency Identification (RFID), grow in popularity. In order to meet the stated requirements, communication nodes and sensors need to become smaller and higher integrated. Focusing on home automation systems, these devices should be secure and cheap to cope with the requirements imposed by the market.

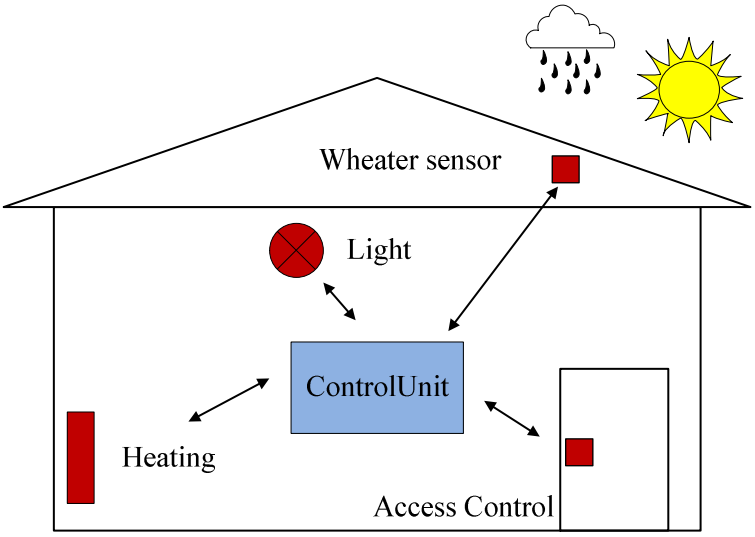

Figure 1.1: Overview of a home automation system connected to a small selection of sensors (red) and a control unit (blue)

A home automation system consists of multiple different elements. Many technical instal-

lations need to be equipped with sensors gathering environmental data. All this data is collected by at least one control unit. Based on the collected information, the control unit makes decisions and initiates actions by sending commands to actuators distributed in the controlled area (Figure 1.1).
So each device of such a system must be able to communicate with the the control unit. To connect all of these components a huge amount of wiring would be needed. This is no problem while the installation is performed during a new home is built, but if existing houses should be upgraded, the expenditure of financial and labour costs would grow significantly high. Additionally, the inflexibility of a wired system makes future extensions extremely difficult.
A wireless home automation system is a possibility to avoid all these disadvantages. Unfortunately many advantages of a wired system also are lost in a wireless system. High speed communication, no interferences and security are the most important ones.
The greatest advantage of wireless communication, the information transport via radio waves, is also the reason for a bigger problem in this scenario. Radio waves will not stop propagating because of a fence surrounding any property. This means, without good secure communication everybody able to use wireless sensing equipment is able to retrieve information from the system. It may seem trivial that, for example, temperature data of any room is not a very sensitive information. But even this information can lead to the conclusion if someone is actually at home or not. Information like this can give an opportunity for persons with any negative intentions to start an incursion. So really every information is private and needs to be protected. To achieve this, in home automation systems an encrypted wireless communication is mandatory.
To establish a secure connection between two devices, the data has to be encrypted with a secret key, transmitted to the second device and decrypted after reception (Figure 1.2). So anybody who is eavesdropping, the transferred data would not get any information out of it. The most vulnerable part of this process is the key exchange between the affected devices. To reduce the risk of leaking the secret keys to a third party, the exchange is done over short range near-field-communication (NFC). This type of wireless connection grants a reading range of some centimeters, so nobody is able to catch the secret key without being detected.

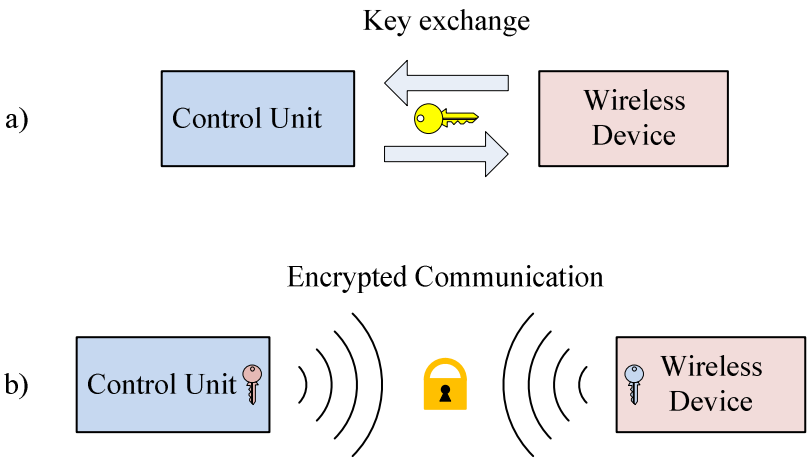

Figure 1.2: Establishing secure communication by firstly exchanging keys (a), and using them to encrypt the data transfer between wireless device and control station (b)

Using these keys, the now encrypted transfer of information and commands between control unit and many peripheral nodes can be accomplished, for example, via long range UHF communication. Therefore, any nodes connected to the home automation system need to have interfaces for both, short and long range communication.
As mentioned above, a home automation system consists of many different wireless devices. Many different products result in higher production costs. The fact that all of these devices should have an equal communication interface, gives the chance for mass production of these parts and reduce costs. Keeping costs low tends to lower product prices and therefore better chances on the market.
As already pointed out, besides of the cost, the size of the products is another issue. Nobody wants to live in a place decorated with well visible electronic devices, distributed in all areas. For wireless devices and interfaces the space required by the antennas is significantly contributing to the size of the product. By shrinking the size of the antenna an important step in lowering the dimension of the products can be accomplished. To achieve this goal, it is important to think about using new packaging technologies to improve integration of electronic elements and combine them with the antenna. This approach would result in wireless devices with significant reduced size.
Considering all of these aspects, we need small, cheap and secure components for successfully designing a marketable home automation system.

In this master thesis a wireless sensor node for a home automation system is designed. The focus of the work is put onto design and simulation of different miniaturized antennas

for the communication interfaces. Here, all design aspects, including the requirements mentioned above, are described.
As a preparation and further understanding the basic antenna and Radio Frequency (RF) theory is introduced before the design process is explained. In this context information on the behavior of radio waves as well as antenna design is presented.
A novel packaging technology, the embedded wafer level ball grid array (eWLB), is introduced. This technology has the potential of high integration of whole systems on a small area and provides the miniaturization needed for our sensor node.
Having this complete information the details of the system setup for the wireless interface of a sensor node is introduced. An overview discusses the main units of the node:

- Microchips used in system
- Intercommunication
- UHF Interface for long range communication
- HF Interface for short range communication

Thereafter, the antenna design section describes the development of the UHF and HF antennas connected to the interfaces, whereas the focus falls onto UHF antenna design. For meeting the restrictions of a very small sensor node planar antennas are investigated. Evaluating the performance of the considered approaches, the corresponding antenna designs were simulated. Based on the results the ones with the highest performance were selected.
The sensor node is constructed on a printed circuit board (PCB) and enclosed to a eWLB package, respectively. Therefore, the design of the circuitry for the microchips was combined with the matching network for the different antennas. All modules were laid out and multiple prototypes were produced. A firmware for the controller was written to test the functionality of the system.
The antenna behavior was characterized by basic parameters measurement. Based on this characterization and further analysis, a conclusion on system applicability and future perspectives was performed.

Chapter 2

Theory

2.1 Circuit Theory

Matching

For efficient transport of the power, generated by a transmitter, to any possible load, transmission lines are needed. But before we discuss transmission lines, we first need to understand how to provide maximum power transfer from a generator to a load. This is even more important in mobile applications were power is usually very limited. Hence, delivering most of the available power to the load (e.g. an antenna or the low noise amplifier) is preferred. Figure 2.1 presents a generator with input impedance Z_G driving a load Z_L.

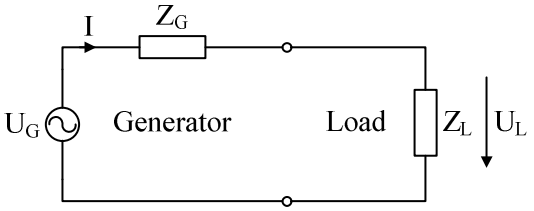

Figure 2.1: Simple schematic with generator and load

The power provided by the generator and dissipated by the load is given by

$$P_{\text{Load}} = \frac{1}{2} Re\left\{U_L I^*\right\} = \frac{|U_G|^2}{2} \frac{Re\left\{Z_L\right\}}{|Z_L + Z_G|^2} = \frac{|U_G|^2}{2} \frac{Z_L + Z_L^*}{(Z_L + Z_G)(Z_L + Z_G^*)} \tag{2.1}$$

$$\frac{\partial P_{\text{Load}}}{\partial Z_L} = \frac{|U_G|^2}{2} \left[\frac{1}{|Z_L + Z_G|^2} - \frac{Z_L + Z_L^*}{|Z_L + Z_G|^4} (Z_L + Z_L)^* \right] =! \, 0 \tag{2.2}$$

$$\rightarrow \frac{1}{|Z_L + Z_G|^2} = \frac{Z_L + Z_L^*}{|Z_L + Z_G|^4} (Z_L + Z_L)^* \tag{2.3}$$

$$\rightarrow |Z_L + Z_G|^2 = (Z_L + Z_G)(Z_L - Z_G)^* = (Z_L + Z_G)^*(Z_L - Z_G)^* \tag{2.4}$$

$$Z_L + Z_G = Z_L + Z_L^* \tag{2.5}$$

$$Z_G = Z_L^* \tag{2.6}$$

For maximum power transfer the load impedance Z_L and the internal impedance of the generator Z_G have to be conjugate complex. This procedure is called matching[4].

$$Z_L = Z_G^* \tag{2.7a}$$

$$R_L = R_G \tag{2.7b}$$

$$X_L = -X_G \tag{2.7c}$$

This model shows that maximum power transfer in a system, shown in Figure 2.1, means that half of the power is dissipated at both the internal resistance of the generator and the load.
In Figure 2.1 the load is connected directly to the generator. This is precise enough, if the the physical distance is small in terms of wavelength. If the wire length between generator and load exceeds about 10 % of the wavelength (Figure 2.2), an additional model for the transmission line has to be used. The transmission line is split into infinite small segments with equal properties. Each of these 2-port networks shown in Figure 2.3, represent a part of the equivalent circuit of a homogeneous line.

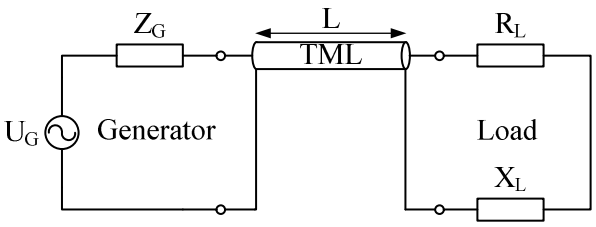

Figure 2.2: Simple circuit where generator and load are connected through a transmission line

The necessity of the transmission line model is caused by the fact that the behavior of lines changes with increasing frequencies. Additionally to resistive losses, the impact of frequency dependent elements, like inductors and capacitors, grows significantly.

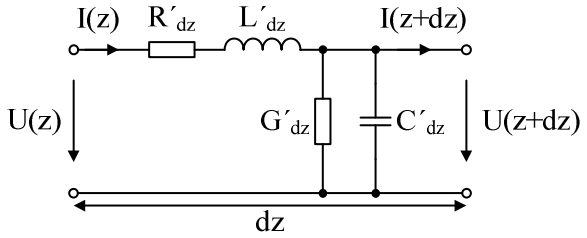

Figure 2.3: Transmission line model of a homogeneous line in z-direction

R'_{dz} = resistance per unit length of the transmission line $[\Omega/m]$
L'_{dz} = inductance per unit length of the transmission line $[H/m]$
G'_{dz} = resistive and polarization losses between conductors because of insulation insufficiency $[S/m]$
C'_{dz} = parasitic capacity between conductors $[F/m]$

Assuming these transmission line segments are infinitely small, the limit of dz is going towards zero; this model leads to a partial differential equation model known as *Telegrapher's equations* [5]:

$$\frac{\partial u(z,t)}{\partial z} + R'i(z,t) + L'\frac{\partial i(z,t)}{\partial t} = 0 \tag{2.8a}$$

$$\frac{\partial i(z,t)}{\partial z} + G'u(z,t) + C'\frac{\partial u(z,t)}{\partial t} = 0 \tag{2.8b}$$

For the sinusoidal steady-state condition these relationships simplify to

$$\frac{dU(z)}{dz} = -(R' + \jmath\omega L')I(z) \tag{2.9a}$$

$$\frac{dI(z)}{dz} = -(G' + \jmath\omega C')U(z) \tag{2.9b}$$

and are solved to

$$\frac{d^2U(z)}{d^2z} - \gamma^2 U(z) = 0 \tag{2.10a}$$

$$\frac{d^2I(z)}{d^2z} - \gamma^2 I(z) = 0 \tag{2.10b}$$

where γ is designated as the *propagation constant*. This is a complex quantity which describes changes of amplitude and phase of an electromagnetic wave during propagation. It is dependent on the material and the geometry of the waveguide.

$$\gamma = \alpha + \jmath\beta = \sqrt{(R' + \jmath\omega L')(G' + \jmath\omega C')} \tag{2.11}$$

α = attenuation constant
β = phase constant

The solution approach for the traveling waves are given by

$$U(z) = U^+ e^{-\gamma z} + U^- e^{\gamma z} \tag{2.12a}$$
$$I(z) = I^+ e^{-\gamma z} + I^- e^{\gamma z} \tag{2.12b}$$

These equations consist of a forward and a backward traveling wave in z-direction. U^+ and I^+ are the amplitudes of waves traveling to the load. The U^- and I^- represent waves running backwards to the generator [6].
By transforming equation 2.9a to

$$I(z) = -\frac{1}{R' + \jmath\omega L'} \frac{dU(z)}{dz} \tag{2.13}$$

and substituting $U(z)$ under derivative with equation 2.12a, it gives

$$I(z) = -\frac{1}{R' + \jmath\omega L'}(-\gamma)(U^+ e^{-\gamma z} - U^- e^{\gamma z}) \tag{2.14}$$

Combining this with equation 2.11, the dependency of current on voltage is shown as:

$$I(z) = \sqrt{\frac{G' + \jmath\omega C'}{R' + \jmath\omega L'}}(U^+ e^{-\gamma z} - U^- e^{\gamma z}) \tag{2.15}$$

The inverse of the square root expression is called the *characteristic impedance* Z_0 of the transmission line [6]:

$$Z_0 = \sqrt{\frac{R' + \jmath\omega L'}{G' + \jmath\omega C'}} = \frac{U^+}{I^+} = \frac{-U^-}{I^-} \tag{2.16}$$

With Z_0 defined, equation 2.12b can be rewritten and the line equations for the current and voltage wave (2.12a) are given[6]:

$$U(z) = U^+ e^{-\gamma z} + U^- e^{\gamma z} \tag{2.17a}$$
$$I(z) = \frac{1}{Z_0}(U^+ e^{-\gamma z} - U^- e^{\gamma z}) \tag{2.17b}$$

The general model described above leads to a complex propagation constant and therefore complex characteristic impedance. A simplification of this model by neglecting the losses of a transmission line results in the loss-less line. This model is usable for many practical cases, because the losses R' and G' on the line are normally very small compared to $\omega L'$ and $\omega C'$. By setting R' and G' in equation 2.16 to zero the characteristic impedance

simplifies to [5]:

$$Z_0 = \sqrt{\frac{\jmath\omega L'}{\jmath\omega C'}} = \sqrt{\frac{L'}{C'}} \tag{2.18}$$

and the propagation constant 2.11 reduces to

$$\gamma = \alpha + \jmath\beta = \jmath\omega\sqrt{L'C'} \tag{2.19}$$

because the attenuation constant α is zero. Hence, both of these quantities are real numbers on a loss-less line.

Reflection Coefficient and Input Impedance

The reflection coefficient Γ is the proportion of backward and forward traveling wave. The reflection coefficient is a complex quantity, containing magnitude and phase information. At a reflection coefficient $|\Gamma| = 1$, the whole wave is reflected to the generator; and $\Gamma = 0$ means that no backward traveling wave exists.

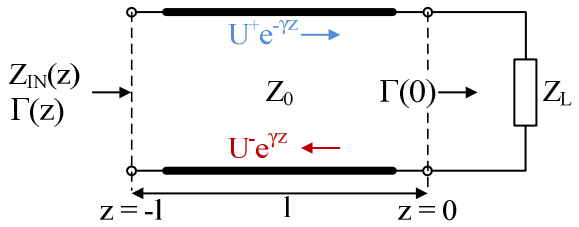

Figure 2.4: Input resistance $Z_{IN}(z)$ and reflection coefficients Γ at entrance and end of the transmission line

The load impedance at the end of the line in Figure 2.4 where $z = 0$, according to equations 2.12a and 2.17b is described by [5]:

$$Z_L = \frac{U(0)}{I(0)} = \frac{U_0^+ + U_0^-}{U_0^+ - U_0^-} Z_0 \tag{2.20}$$

The reflection coefficient Γ_0 at $z = 0$ therefore is

$$\Gamma_0 = \frac{U_0^-}{U_0^+} = \frac{Z_L - Z_0}{Z_L + Z_0} \tag{2.21}$$

and out of 2.12a for

$$\Gamma(z) = \frac{U^-(z)}{U^+(z)} = \frac{U_0^- e^{\gamma z}}{U_0^+ e^{-\gamma z}} = \Gamma_0 e^{2\gamma z} \tag{2.22}$$

The voltage and current at the input of the line can be rewritten to

$$U(z) = U_0^+(e^{-\gamma z} + \Gamma_0 e^{\gamma z}) \tag{2.23a}$$

$$I(z) = \frac{U_0^+}{Z_0}(e^{-\gamma z} - \Gamma_0 e^{\gamma z}) \tag{2.23b}$$

Out of Equation 2.21 it turns out, with $Z_0 = Z_L^*$ the reflection coefficient becomes zero. With Γ different to zero a superposition of transmitted and reflected wave occurs and a so called standing wave arises (Figure 2.5).
Out of this we finally get the *transmission line impedance equation* and consequently the input impedance of the line:

$$Z_{\text{IN}}(z) = \frac{U(z)}{I(z)} = Z_0 \frac{1 + \Gamma_0 e^{2\gamma z}}{1 - \Gamma_0 e^{2\gamma z}} = Z_0 \frac{Z_L - Z_0 \tanh(\gamma z)}{Z_0 - Z_L \tanh(\gamma z)} \tag{2.24}$$

This important equation shows that the input impedance Z_{IN} no longer depends on the length of a loss-less transmission line if the load is matched to the line.

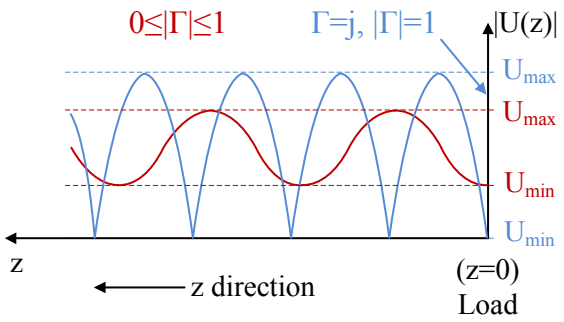

Figure 2.5: Voltage distribution on a line at different values $\Gamma = 1$ and $\Gamma > 0$

Return Loss

If the load is mismatched, only a part of the power provided is delivered to the load. This so called return loss is defined as:

$$RL(dB) = 10 \log \frac{P_i}{P_r} = -20 \log |\Gamma| \tag{2.25}$$

RL = return loss [dB]
P_i = incident power
P_r = reflected power

A matched load with $\Gamma = 0$ has a return loss of ∞ dB; no power is reflected. On the other hand at full reflection $\Gamma = 1$ the return loss is 0 dB [5]. A large return loss indicates that the reflected power is small in comparison to incident power. The higher the return loss the better the matching.

Voltage Standing Wave Ratio VSWR

Another figure of merit for mismatching is the voltage standing wave ratio. A reflected wave, caused by a mismatch, adds up with the incident wave resulting in a standing wave on the transmission line. Hence, the magnitude of the voltage across the line is not constant.
The corresponding maximum and minimum voltages are given by [5]

$$U_{\max} = \left|U_0^+\right| (1 + |\Gamma|) \tag{2.26a}$$
$$U_{\min} = \left|U_0^+\right| (1 - |\Gamma|) \tag{2.26b}$$

The *standing wave ratio* is defined as ratio of $U_{\max}$ to $U_{\min}$.

$$\text{VSWR} = \frac{U_{\max}}{U_{\min}} = \frac{1 + |\Gamma|}{1 - |\Gamma|} \tag{2.27}$$

When $|\Gamma|$ changes, also the ratio between maximum and minimum voltage on the line changes. Figure 2.5 shows the voltage along the transmission line for two different values for the reflection coefficient.

Frequency and Wavelength

The wavelength λ of a sinusoidal wave is defined as the smallest distance between two points of the same phase on a wave. It is dependent on frequency f and propagation velocity. While frequency is constant, propagation or phase velocity v_p is influenced by the environment.

$$\lambda = \frac{v_p}{f} \tag{2.28}$$

and for phase velocity

$$v_p = \frac{1}{\sqrt{\epsilon\mu}} = \frac{1}{\sqrt{\epsilon_0\epsilon_r\mu_0\mu_r}} \tag{2.29}$$

where:

ϵ = absolute permittivity
ϵ_0 = vacuum permittivity
ϵ_r = relative permittivity of the material
μ = absolute permeability
μ_0 = vacuum permeability
μ_r = relative permeability of the material

In vacuum electromagnetic waves travel with the speed of light c.

$$v_{\text{vacuum}} = c_0 = \frac{1}{\sqrt{\epsilon_0 \mu_0}} \tag{2.30}$$

The wavelength λ in vacuum therefore is

$$\lambda_0 = \frac{c_0}{f} \tag{2.31}$$

Using equations 2.29 and 2.30 as well as considering that the value for the relative permeability μ_r of dielectric materials is about 1, the phase velocity results in

$$v_p = \frac{c}{\sqrt{\epsilon_r}} \tag{2.32}$$

This results in the definition of the wavelength for waves propagating in materials different to vacuum:

$$\lambda = \frac{c}{f\sqrt{\epsilon_r}} \tag{2.33}$$

Microstrip Line

A microstrip line is a special transmission line primarily used on printed circuit boards (PCBs) or integrated circuits. It consists of a metal line and a ground plane separated by any dielectric substrate (Figure 2.6).

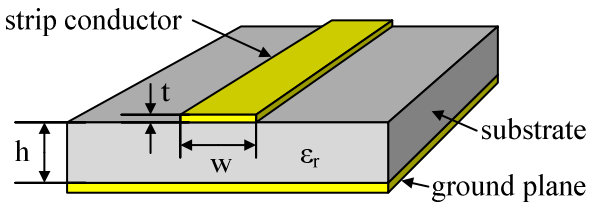

Figure 2.6: Structure of a microstrip line

As mentioned above, wave propagation on transmission lines is effected by the different dielectric media surrounding them. For microstrip lines, the substrate separating the metal line from the ground plane, and the surrounding air add up to an inhomogeneous medium.

This results in field lines in the substrate between the strip conductor and the ground plane as well as field lines in the air above the line [5]. As the permittivity ϵ_r differs between these materials, phase velocity and therefore propagation speed is also different. Therefore, the equations 2.32 and 2.33 can not be used to estimate the corresponding phase velocity v_p and wavelength λ on the line. To overcome this problem, a new quantity, the effective permittivity $\epsilon_{\mathrm{r,eff}}$, is introduced to describe the surrounding environment as a homogeneous medium. The effective dielectric constant for microstrip lines is approximately described by the following equation [5]:

$$\epsilon_{\mathrm{r,eff}} = \frac{\epsilon_r + 1}{2} + \frac{\epsilon_r - 1}{2} \left(1 + \frac{12h}{w}\right)^{-\frac{1}{2}} \tag{2.34}$$

$\epsilon_{\mathrm{r,eff}}$ = effective permittivity
w = width of the microstrip line
h = thickness of the substrate (Figure 2.6)

The phase velocity and wavelength for propagating waves on the microstrip line are then given by replacing the relative permittivity ϵ_r in the equations 2.32 and 2.33 with the newly introduced effective permittivity $\epsilon_{\mathrm{r,eff}}$:

$$v_p = \frac{c}{\sqrt{\epsilon_{\mathrm{r,eff}}}} \tag{2.35}$$

$$\lambda = \frac{c}{f\sqrt{\epsilon_{\mathrm{r,eff}}}} \tag{2.36}$$

2.2 Antenna Parameters

In the following, some fundamentals on antennas will be mentioned. The performance of an antenna is mostly described by the following parameters.

Directivity

The directivity D describes how 'directional' an antenna is. Therefore it is defined as "The ratio of the radiation intensity in a given direction from the antenna to the radiation intensity averaged over all directions" [4]. Where the average radiation intensity is equivalent to the total radiated power divided by 4π. Antennas with omnidirectional radiation pattern, called isotropic antenna, would have a directivity of 1 (0 dB).

$$D = \frac{U}{U_0} = \frac{4\pi U}{P_{\text{radiated}}} \tag{2.37}$$

D = Directivity [dimensionless]
P_{radiated} = total radiated power [W]
U = radiation intensity [W/unit solid angle]
U_0 = radiation intensity of isotropic source [W/unit solid angle]

In Figure 2.7 the radiation characteristics of an isotropic compared to an directive antenna can be seen. This is a simplified diagram in the two dimensional view. The concentric circles represent different power levels, while greater distance to the origin means higher power. The angle indicates the direction of radiation relative to the orientation of the antenna. The blue and red areas represent the power radiated from two different antennas in the given direction. In reality, the radiation pattern of an ideal isotropic antenna would be a sphere, but is simplified and pictured by the blue circle. A real antenna is not able to radiate power uniformly to all directions and, therefore, has an own radiation pattern. In Figure 2.7 the red lobe indicates the power radiated from a directive antenna into a specific direction. In this case, the highest power level is transmitted at an angle of 90°. The radiation characteristic of a passive antenna is usually valid for both transmission and reception.

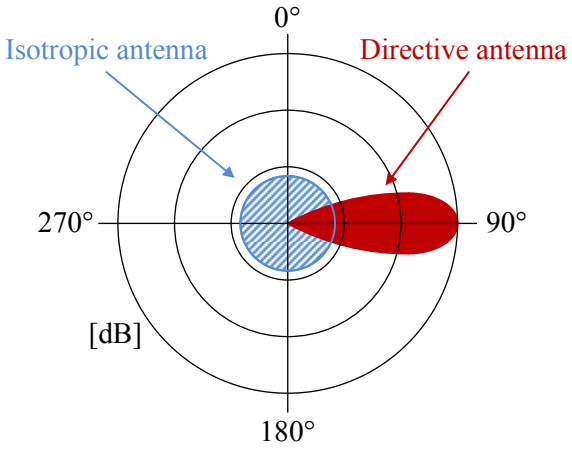

Figure 2.7: Directivity characteristics of an isotropic and directive antenna in a two dimensional view

The logarithmic representation of the directivity D of an antenna is expressed by [4]

$$D_{\text{dB}} = 10\log(\frac{D}{D_{\text{reference}}}) \tag{2.38}$$

$D_{\text{reference}}$ = Directivity of a reference antenna [dimensionless]

The reference antenna is typically an isotropic antenna, which, as mentioned above, has a directivity of 1.

$$D_{\text{dBi}} = 10\log(\frac{D}{D_{\text{isotropic}}}) = 10\log(D) \tag{2.39}$$

Directivity referenced to an isotropic antenna is specified in dBi.

Efficiency

Radiation efficiency is the ratio between power delivered to the antenna and the power radiated. The higher the efficiency, the more energy is radiated. A low efficient antenna absorbs most of the power instead of radiating it. The main reasons for absorptions are the finite conduction of the antenna (conduction loss) and losses in dielectric materials (dielectric loss).

$$e_r = \frac{P_{\text{radiated}}}{P_{\text{delivered}}} \tag{2.40}$$

where e_r defines the radiation efficiency of the antenna. The radiation efficiency is limited to a value between 0 and 1. More often the efficiency is quoted in percent. Generally, the radiation efficiency can be composed from the efficiencies related to the conduction and

dielectric losses.

$$e_r = e_c e_d \tag{2.41}$$

e_r = radiation efficiency
e_c = conduction efficiency
e_d = dielectric efficiency

Further the term for the "total efficiency" e_0 also includes the influences of impedance mismatch [4].

$$e_0 = e_r(1 - |\Gamma|^2) \tag{2.42}$$

Gain

The antenna gain $G(\Theta, \phi)$ is an important parameter that combines directivity and efficiency. Whilee directivity is proportional to the radiation pattern of an isotropic antenna, gain describes the real power radiated direction given by the angles Θ and ϕ.

$$G(\Theta, \phi) = e_r D(\Theta, \phi) \tag{2.43}$$

$G(\Theta, \phi)$ = antenna gain
$D(\Theta, \phi)$ = antenna directivity

If the gain G is given without any sign of a direction, the gain is usually taken in the direction of maximum power radiation [4].

$$G_{\mathrm{dB}} = 10 \log(e_r D) \tag{2.44}$$

Practically the gain is given in decibel [dB].

Near and Far field

The area surrounding an antenna is divided into different regions. As shown in Figure 2.8, the reactive region as well as the so called Fresnel or radiative field region, belong to the near field. The region beyond is defined as far field or Fraunhofer region.
In the reactive near field surrounding the antenna at close distance, reactive fields are dominating. In this region the E- and H-fields are not in phase and can be measured separately. For most antennas the range of the reactive field is given as $R_1 = 0,62\sqrt{D^3/\lambda}$, where D is the largest dimension of the antenna.
The radiating near field is the region between reactive region and far field. In this region the fields begin to radiate. The angular field distribution is dependent on distance to the antenna. If the maximum dimension of the antenna is small compared to wavelength, no

Fresnel region may exist at all. The distance of $R_2 = 2D^2/\lambda$ from the antenna indicates the border between near and far field, which is called Rayleigh distance. Here the angular field distribution is independent from distance to the antenna. The radiating E and H field strength decreases inversely with distance from the antenna. This results in inverse square reduction of the radiation power with increasing distance.

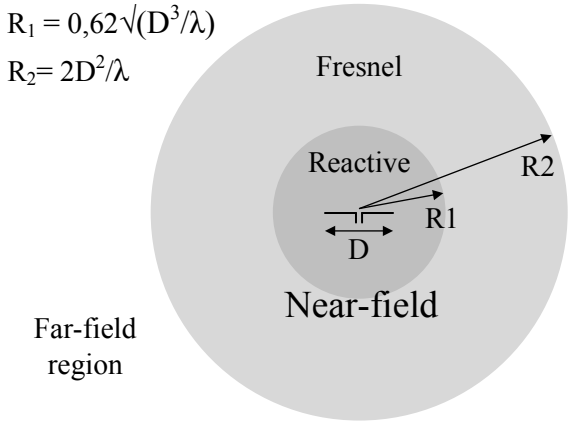

Figure 2.8: Near and Far field regions of an antenna

Antenna Radiation

In the following will be explained how antennas are radiating electromagnetic waves. Generally, radiation of an antenna is caused by accelerated electric charges. This can be imagined like a stone, thrown into a calm lake of water. The stone in this scenario, is actually the accelerated charge causing disturbances when piercing the water surface. It can be observed, that the resulting waves continue propagating, whether the stone lost all acceleration lying on the sea ground and taking a rest. So accelerated charges are responsible for generating radiation, but are not responsible for keeping the wave propagation alive.
On an antenna, oscillating charges travel back and forth between the ends and cause continuous radiation. The frequency of the oscillation thereby determines the frequency of the radiated waves. The principle of antenna radiation is shown in Figure 2.9. The upward flowing current causes a concentration of charges in the upper half of the antenna and lack of charges on the lower half (2.9a). This induces a voltage between the two halves resulting in a current flowing downwards. When the charges have neutralized due to the current flow, no more charges are available to terminate the field lines, which form closed loops near the antenna (2.9b). During the next cycle, negative charges are concentrating at the top of the antenna (2.9c), again establishing a voltage between the two ends. While keeping the antenna fed by an RF signal, electromagnetic waves are radiated continuously [1].

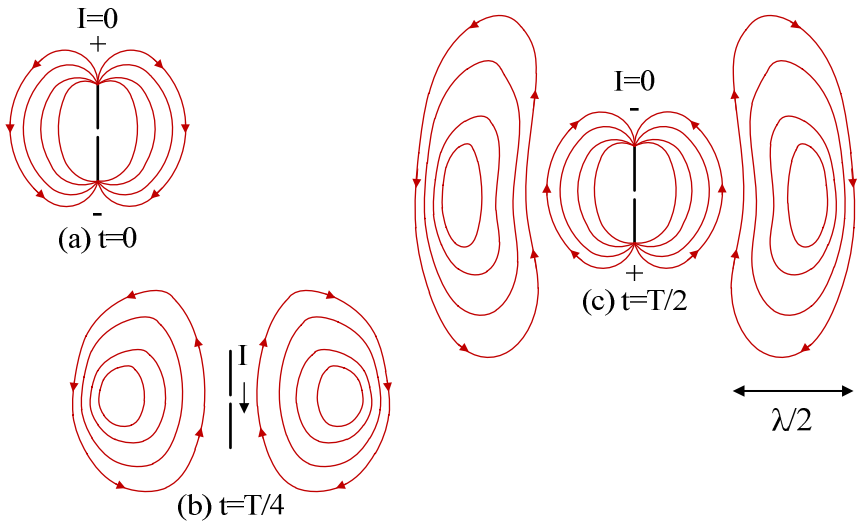

Figure 2.9: Fields of an oscillating charge dipole for different instants of time [1]

Antenna Impedance

In this master thesis an antenna is representing the load, described in the previous chapter. Hence, to match the antenna to the generator, the antenna impedance has to be defined. But first, let us define what an antenna really does. An antenna acts as impedance transformer between transmission lines and the free space. The *impedance of free space* is a physical constant, relating the magnitudes of the electric and magnet fields of electromagnetic waves travelling through free space.

$$Z_{\text{free space}} = \frac{E}{H} = \mu_0 c_0 = \sqrt{\frac{\mu_0}{\epsilon_0}} \approx 377\Omega \tag{2.45}$$

E = electric field strength
H = magnetic field strength
μ_0 = vacuum permeability
ϵ_0 = vacuum permittivity
c_0 = speed of light in free space

The type and design of an antenna allows us to make it a good transformer to free space. On the other side this also results in an input impedance at the terminals of the antenna. This is defined as "the impedance presented by an antenna at its terminals or the ratio of the voltage to current at a pair of terminals or the ratio of the appropriate components of the electric to magnetic fields at a point" [4].

The impedance at the input terminals of an antenna Z_A consists of real and imaginary part.

$$Z_A = R_A + jX_A \tag{2.46}$$

where the real part can be divided into the radiation resistance R_r and a loss resistance R_L which combines all losses in the antenna. The radiation resistance is used to represent the power delivered to the antenna for radiation.

$$R_A = R_r + R_L \tag{2.47}$$

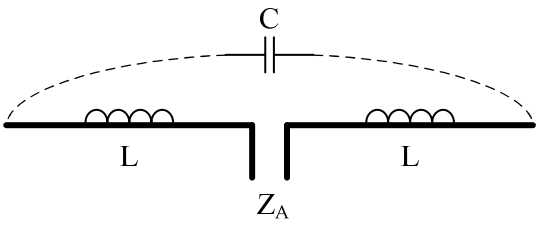

Figure 2.10: Reactive elements of a dipole antenna

The reactive elements of the antenna impedance arise from the fact that an antenna acts as a tuned circuit which consist of inductance and capacitance (Figure 2.10). Most antennas are operated at resonance where inductance and capacitance cancel out.
As mentioned above, the antenna acts as load at the end of a transmission line. Referring to Chapter 2.1 the impedance has to be matched to the transmission line to avoid reflections.

2.3 Antenna Types

There are many different types of antennas available for wireless devices. The most common types are the so called wire antennas. Low cost and simple design make them a good choice for many applications. Another type described below are Patch antennas. Their low profile combined with easy and cheap fabrication makes them an ideal solution for mobile wireless devices. These two antenna families are described in more detail in the following sections.

2.3.1 Wire Antennas

As the name tells, wire antennas consist mostly of one ore more wires. The two ends of a symmetrical transmission line bent perpendicular to the line would be a dipole. While single radiating wire end acts as a monopole.

Dipole

The dipole antenna especially the half-wave dipole is a very popular antenna (Figure 2.11). This type of antenna is realized as a straight wire fed in the center. The radiation pattern of half-wave dipole is donut or torus shaped. Figure 2.11 shows the current distribution on a dipole, where the red wave depicts a full-wavelength dipole and the blue one the half-wave dipole. The wave on the antenna is sinusoidally oscillating in time at the frequency f.

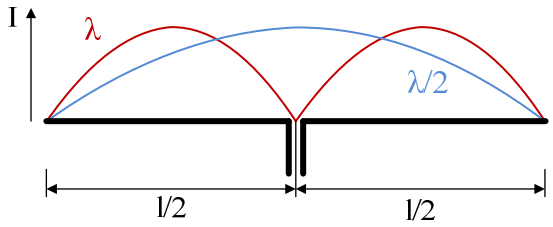

Figure 2.11: Current distribution on a dipole antenna for different dipole length l

The input impedance of an infinitely thin half-wave dipole is $Z_{\mathrm{A,dipole}} = 73 + j42.5\,\Omega$ [1]. Getting this antenna resonant in case of eliminating the reactance is pretty simple: the wire ends need to be trimmed. An antenna size of about 0.48λ the input impedance of the tuned dipole is $Z_a = 70 + j0\,\Omega$. Another way to reach this goal is thickening the wire which in addition leads to increased bandwidth. Because this value is very close to the characteristic impedance of most common devices ($50\,\Omega$) there is no need for a matching network.

Monopole

The monopole antenna is dipole antenna cut into half at its center feed point. Using image theory, the monopole antenna over a perfect ground plane behaves like a dipole antenna

in free space (Figure 2.12). The radiation pattern of the monopole is the same as a dipole but radiating only half of the power. As seen in Equation 2.48 this leads to a doubling of the directivity [1].

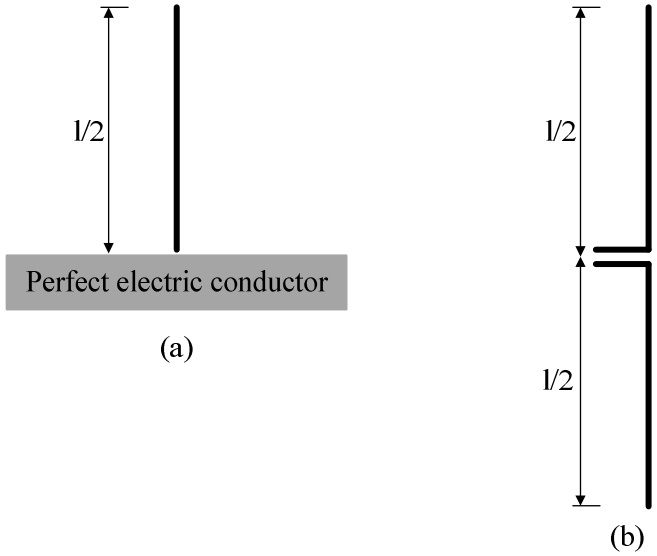

Figure 2.12: Monopole antenna over a perfect ground plane (a), and the equivalent dipole in free space (b)

$$D_{\text{monopole}} = \frac{4\pi U}{\frac{1}{2}P_{\text{radiated}}} = 2D_{\text{dipole}} \tag{2.48}$$

The input impedance of a quarter-wave monopole is [1]

$$Z_{\text{A,monopole}} = \frac{U_{\text{A,monopole}}}{I_{\text{A,monopole}}} = \frac{\frac{1}{2}U_{\text{A,dipole}}}{I_{\text{A,monopole}}} = \frac{1}{2}Z_{\text{A,dipole}} = 36 + j21.3\,\Omega \tag{2.49}$$

2.3.2 Patch Antennas

The patch or microstrip antenna is a printed planar antenna which is constructed similarly to printed circuit boards. This simple assembly and the consequential low costs are the great benefits of these types of antennas.
Figure 2.13 shows a simple patch antenna. It behaves similar to an ordinary microstrip line. The difference is the rectangular patch designed for radiating electromagnetic waves. The wave is traveling along the transmission line (TML) to the patch. An electric field arises between the microstrip and the ground plane, oscillating with the frequency of the standing wave on the patch. The fringing fields at the edges of the patch are responsible for radiation. The field lines are bended between the ends of the patch antenna, uncouple from the into free space [7].

With changing the length L of the patch, the resonant frequency of the antenna can be adjusted. The parameter W, the width of the patch, is responsible for the impedance of the patch antenna.

$$f = \frac{c}{2(L+h)\sqrt{\epsilon_{\text{eff}}}} \tag{2.50}$$

The thickness h of the dielectric material is often very small compared to the length L and is sometimes neglected.

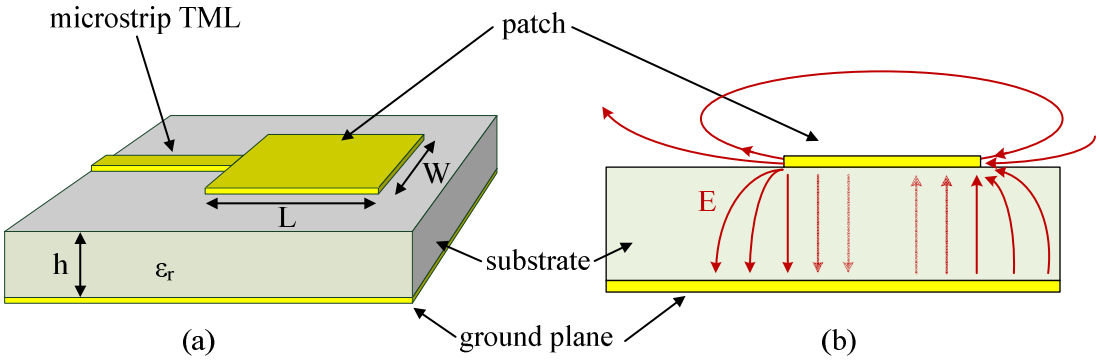

Figure 2.13: Patch antenna with feed line (a), and a cross section of the antenna showing the electric field (b)

The current and voltage distribution is 90° out of phase to each other. Though the patch acts like a transmission line with an open end, the current is zero at the edges and maximum in the middle. The voltage distribution is exactly opposite and is at maximum at the edges and zero in the center of the patch. Out of that the input impedance is theoretically infinite. In reality it is about 400 Ω. To get rid of reflections if for example using a 50 Ω transmission line, the feed point is moved further into the patch.

Inverted F Antenna

The inverted F antenna is the product of some iterative modifications of a quarter wave monopole. The first step is to bend a quarter wave monopole over a ground plane. Because of the resulting shape of this type of antenna, it is called inverted L antenna. The advantage of the inverted L antenna is the higher compactness compared to the monopole, but it still has a very low input impedance (2.49). To get rid of this drawback, a shortcut arm is added to the radiating element which leads to the inverted F antenna (Figure 2.14), where the name also refers to the shape of the antenna. This shortcut acts as inductance in transmission line theory and changes the input impedance of the antenna. By changing the distance of the shortcut to the feed, the antenna can be matched to a transmission

line without any matching network [8].

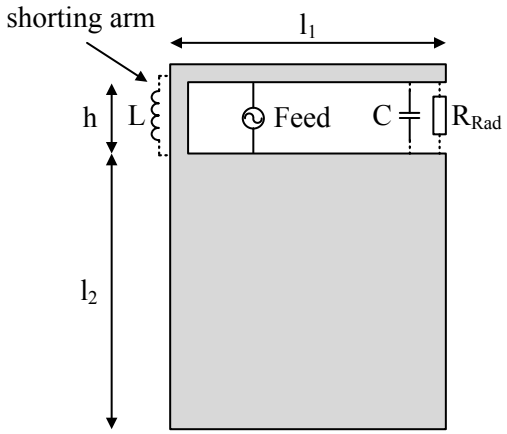

Figure 2.14: Schematic structure of a printed Inverted F antenna. The capacitor C and inductance L represent the equivalent elements of a transmission line model

Loop Antenna

The printed resonant loop antenna described here is actually a folded dipole with a T-matching structure. The wings of the dipole are folded in the shape of a loop leaving a small gap at there meeting point, which acts as a capacitor (Figure 2.15). With changing the gap size, the resonant frequency of the antenna can be adjusted. The shortcut between the feed point and ground acts as an impedance transformer [9]. By moving the GND connection, the impedance of the antenna is changed and therefore can be matched without any further matching structure.

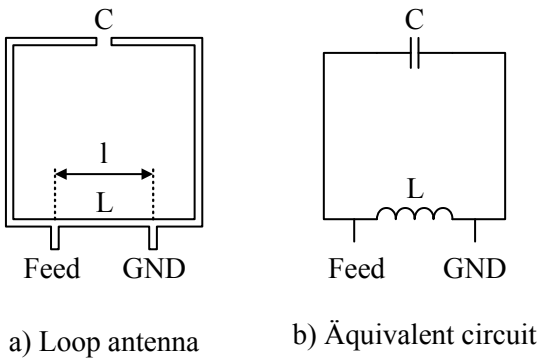

Figure 2.15: Schematic structure of the printed loop antenna (a) and the equivalent circuit (b)

This antenna is not used very often as a transmitting antenna because the efficiency of this design suffers very much from reduced antenna area, however, it is chosen because of the possibility of matching without any additional matching network.

2.4 The Smith Chart

The Smith Chart (Figure 2.16) is a graphical utility, developed in 1939 by P. Smith, which is very useful for graphically solving transmission line and matching problems.

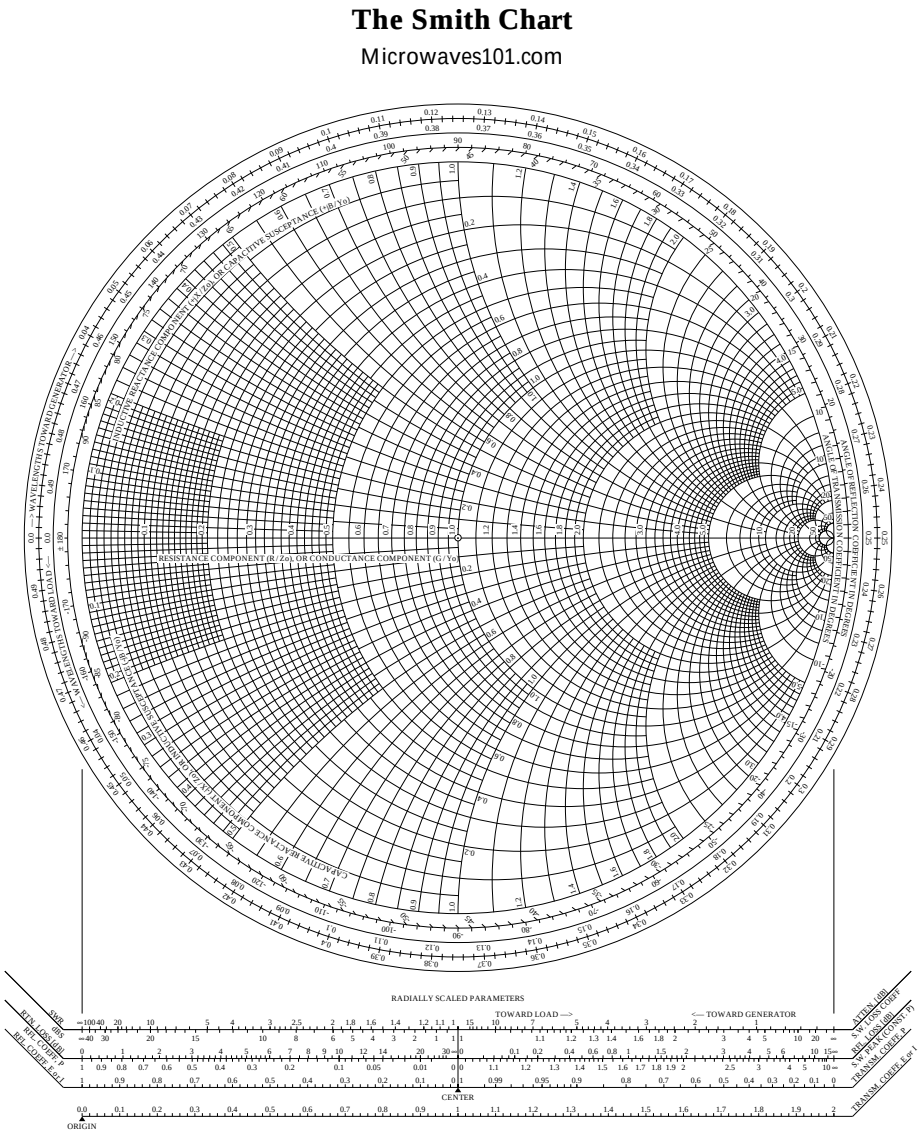

Figure 2.16: The Smith Chart

It represents the right part of the complex impedance or admittance plane mapped into the unit circle. The left side is outside of the smith chart circle and is used for designing active devices, because it corresponds to negative resistances. The Smith Chart can be used to display multiple parameters like impedance, admittance and reflection coefficient, etc. [5].
The reflection coefficient in polar coordinates looks like:

$$\Gamma = |\Gamma| \, e^{j\varphi} \tag{2.51}$$

Where the magnitude $|\Gamma|$ is plotted as the radius ($|\Gamma| \leq 1$) of the unit circle and the angle φ ($-180° \leq \varphi \leq +180°$) is measured counterclockwise from the horizontal diameter on the right side (Figure 2.17) [5]. The value of the reflection coefficient in the center of the circle is zero.

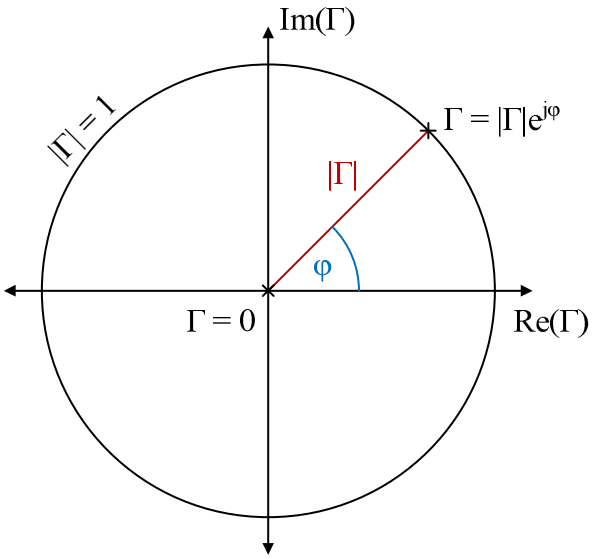

Figure 2.17: Graphical representation of the reflection coefficient in the smith chart

Generally, when working with impedance, all values are normalized, using the characteristic impedance as normalization constant $z = \frac{Z}{Z_0}$. Hence, every reflection coefficient plotted on the Smith chart can be converted into normalized impedance and vice versa.
Impedance are plotted using the resistance circles and reactance curves shown in Figure 2.18. Every circle or curve represents a specific value for resistance or reactance. Following the circles to the horizontal axis, the value can be read off. The very left point on the diameter is the short circuit point, the impedance at this point is $z = 0$. At the center, $z = 1$, the impedance is matched. The impedance at the far right point is infinite and called the open circuit point. The reactance values along the curves are shown at the outer boundary of the Smith Chart.

Like in the complex plane, the imaginary part of the impedance is positive (inductive) in the upper half, and negative (capacitive) in the lower half. Instead of impedance also admittances can be plotted in the Smith Chart. In this case the circles and curves are mirrored at the horizontal diameter [5].

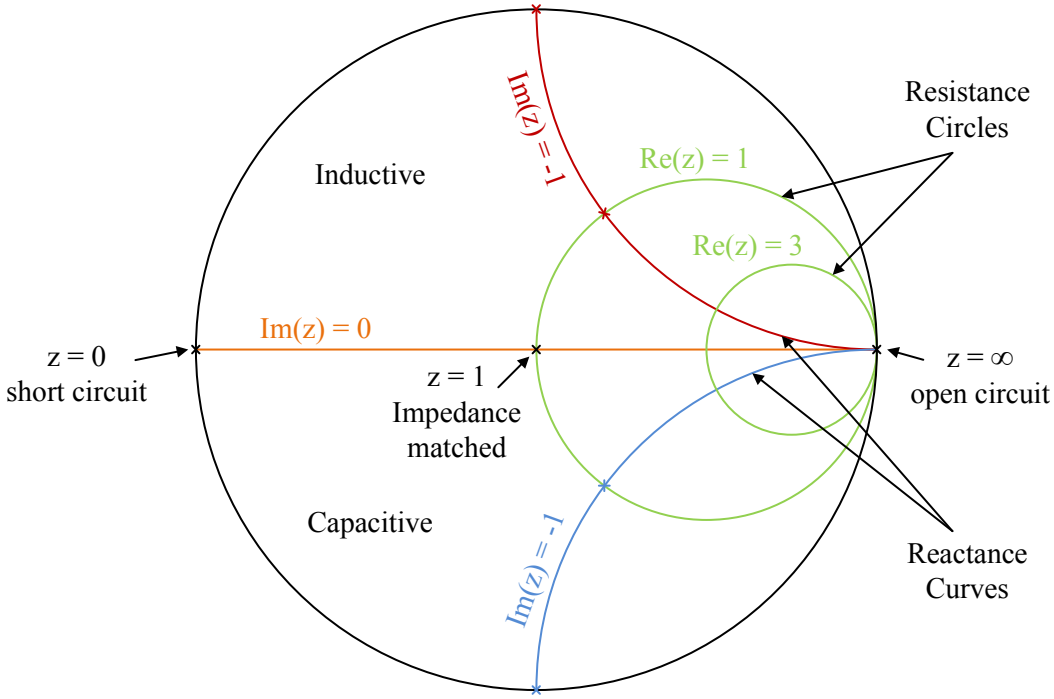

Figure 2.18: Impedance representation on the Smith Chart

Rotating around the center of the Smith Chart describes the effect when moving along a transmission line. The angle between two points on this circle represents the distance on the transmission line, in terms of wavelength fractions. A transmission line length of $\frac{\lambda}{2}$ corresponds to a full rotation around the circle. Additionally, the direction of the rotation is important. Clockwise rotation implies movement towards the generator, while counterclockwise means moving towards load.
Nowadays the original purpose of the Smith Chart, of simplifying complex calculations by doing it the graphical way, was diminished because of powerful calculators and computers. But it is still one of the preferred options to represent and understand the behavior of transmission lines without the need of detailed calculations.

Chapter 3

Embedded Wafer-Level Ball Grid Array

The embedded Wafer-Level Ball Grid Array (eWLB) technology is an innovative packaging technology developed during recent years. A System in Package (SiP) combines multiple electronic components of different functionality in a single package [2]. This provides much flexibility in designing new systems for a huge number of applications. SiP was developed as an alternative to the System on Chip (SoC) integration technology because it gives some advantages compared to SoC. System in Package offers high integration flexibility with faster time to market at lower R&D costs. On the contrary, System on Chip is more suitable at high volume applications because of higher integration ability [2]. However, only after calculating all costs including chip areas, yield costs, test costs, assembly and packaging costs, it can be determined, which approach gives the lowest product cost.
The classic System in Packages can be divided into three major categories:

- Stacked Die Packages
- Stacked Package-on-Package (PoP)
- Multi-Chip Package (MCP)

Any package with more than two vertically stacked chips are called Stacked Die Packages. The dies are interconnected in the package and mounted on a substrate. This type of SiP is mainly used for memory stacks.
In this technology wire bonding is still the typical way of connecting the chips. The limitations of wire bonding are bypassed in developing new approaches including thin film technology redistribution and through silicon vias (TSV). TSVs provide shorter and more robust interconnections inside the package. This allows thinner packages, higher integration density and higher performance. TSVs are the most advanced technology for die stacking, but still are very expensive compared to other solutions [2].
Package-on-Package consist of multiple pre-packed chip dies stacked upon each other. All single packages, which are usually pre-tested PCB or wafer level packages, are intercon-

nected to the packages above and below. The greatest advantage of PoP is the possibility of testing the single packages before stacking. The typical structure consists of a bottom package containing a high performance device carrying one or more top packages above. The top packages usually consist of a memory device or a stack of memory devices. The advantage of PoP is the greater flexibility in selecting the top packages. They can more easily exchanged during development than chip dies in other package technologies. The biggest disadvantage are the longer connections from bottom to top of the package compared to stacked die packages [2].
Stacked Packages have their great advantage in size reduction due the $3D$ approach, and are already used in mass production. These two mentioned technologies differ in their pros and cons. PoP give a greater flexibility, better testability and reworkability at higher cost and greater package profile. Die stacking comes with a lower profile due possible use of advanced wafer thinning technology and very small substrate consumption. Reworking of stacked die packages is nearly impossible and needs new development for changing a elements in the stack.
Multi-Chip Packages are fully functional subsystems consisting of multiple chip dies, positioned side by side. They can also include additional passive components. The dies are usually wire bonded or mounted in flip chip technology. MCPs are similar to classical Ball-Grid-Array (BGA) chip packages, simply with more components inside. The integration density of MCPs is not very high, as all integrated components nearly need the same space on a printed circuit board (PCB) if mounted without the package. Therefore they are used for applications where space is not the biggest problem. But the high flexibility in usable base materials, functionality and the low time to market, show the advantages of this approach [2].

The newest MCP approach are Wafer Level Packaging (WLB) technologies, especially the fan-out WLB. One of these is the embedded Wafer Level Ball Grid Array (eWLB), which was developed and introduced by Infineon [2]. The eWLB technology allows minimal package size without need of an interposer due thin film technologies, at excellent electrical performance. All known Wafer Level technologies have some points in common:

- a pin-out redistributed from the pads to an area array
- a vertical element used for second level assembly
- the package is fully processed on a wafer
- the resulting package is of chip size; all connection pins have to fit under the die

The greatest restriction for Wafer Level Packaging is the fact, that chip trend to smaller size at increasing number of pads for interconnection. So more connections are needed on the bottom surface of the package. Pitches and pads on the chip are much smaller than on package and board interface, so a so called interconnection gap emerges (Figure 3.1).

To overcome this problem, fan-out packaging is required where the package size is larger than the chip, to provide area for the interconnects for second level assembly [2].

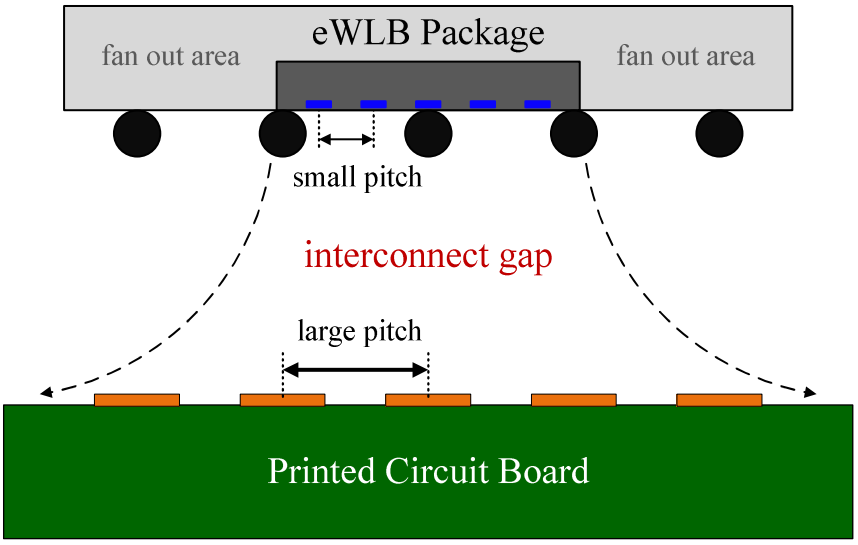

Figure 3.1: Interconnection gap between package and printed circuit board [2]

With the eWLB technology, it is possible to realize any number of interconnections with standard pads at any shrink stage of silicon wafer technology. The area around the chip die, called fan out area, grants the needed space for interconnections as seen in Figure 3.1. This fan out area is highly flexible in its dimensions and can also be used for other functional elements in the package. Metal layers inside the package are used to connect electrical elements. These layers can also be used to design small antennas inside the eWLB. This allows to realize small autonomous nodes. In applications like RFID, units can be implemented without any further assembling [10].

3.1 Internal Structure and Process Flow of eWLB

The integration of all components occurs on an artificial wafer called Reconstitution. The sequence of the production process is shown in Figure 3.2 [3]. First, a temporary metal layer and an adhesive tape are combined (a). The chip dies are flipped and placed on the tape (b). The technology also allows to stack chips, not only put them side by side. A minimum distance between the dies has to be kept. The placing of the chips defines the fan out area which in this application is used for an antenna. The area around the chips is filled with a liquid mold compound (c). This provides the structural integrity of the eWLB. After this, the package is released from the subcarrier (d). The molded Reconstitution Wafer now forms the base for the further steps. The bottom of the eWLB is now coated with a dielectric layer (e). After that the thin-film metal layer called redistributon is

applied (f). This layer is also used for antenna designs. Another dielectric layer is applied onto the redistribution layer (g). For further connections to external circuits like a PCB, solder balls are connected to the package (h). After that, the waver is laser cut and the eWLB packages are ready to use [2].

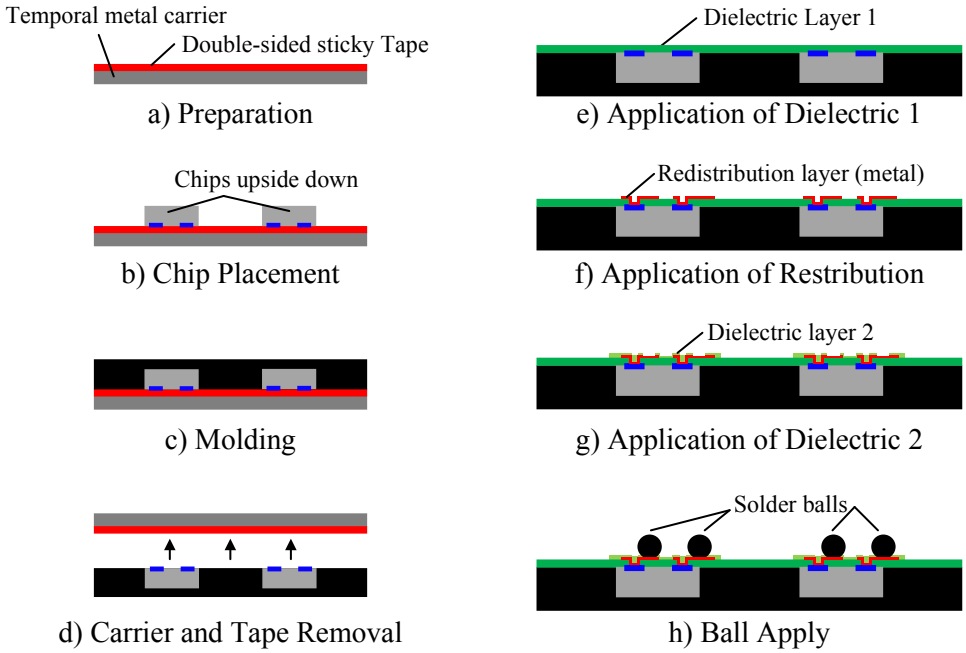

Figure 3.2: Production process of eWLB [3]

3.2 Design Restrictions

Due to the eWLB manufacturing process and the requirements of the targeting application, restrictions are imposed to the antenna design derived in this thesis. The design of a sensor node for the UHF band demands antennas with adequate size. Miniaturization of antennas implies reduction in efficiency and therefore communication range. To ensure structural integrity of the eWLB package, the size is limited which results in a great challenge in antenna design. Another problem is the inaccessibility of single components in the high miniaturized package. This means, tuning of the antennas, after the package is produced, is nearly impossible. To approve functionality of the antennas, their prior simulations have to be very exact. To achieve this, an exact model of the eWLB composition, for the large number of different materials, used in this technology, is needed.

Chapter 4

System Overview

The focus of this chapter is on the detailed description of the developed wireless sensor node. As mentioned in Chapter 1 a wireless sensor node for a home automation system requires at minimum two interfaces to provide secure communication. One short range interface for programming the node as well as for exchanging security keys with the control unit. In a secure system, the sensor data and commands from the control unit are encrypted with the security keys exchanged before, and transmitted over a long range interface. The security mechanism itself is explained in detail in [11].

4.1 System Description

In Figure 4.1 the structural design of the sensor node is represented.

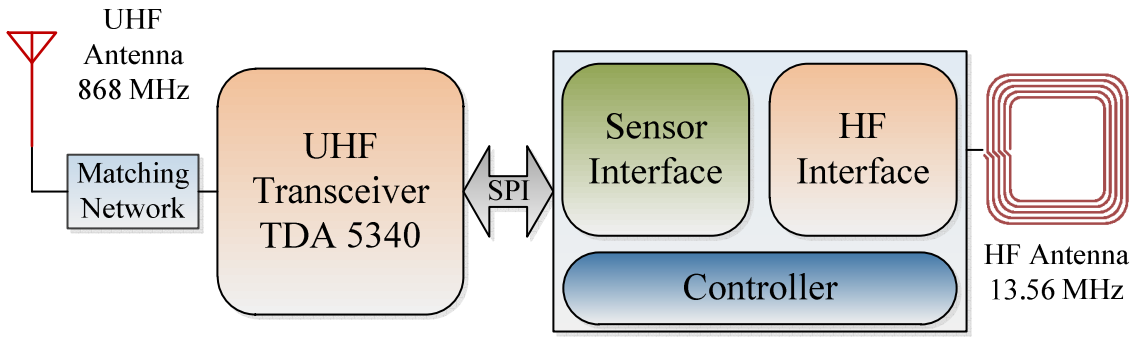

Figure 4.1: Block diagram of the whole wireless sensor node

The system in general consists of the following elements:

- ASIG: main controller, sensor interface and HF communication

- Transceiver chip TDA5340 for UHF communication
- UHF antenna for long range communication (868 MHz)
- Matching network for UHF antenna
- HF antenna for near field communication (13.56 MHz)
- Power supply circuitry

ASIG, an experimental chip developed by Infineon, acts as main controller of the sensor node. The ASIG consists of an integrated microcontroller, a sensor interface and a HF interface for near field communication. Power supply for the chip can be set up via the HF interface or the standard power pin.
The chip is able to communicate over an Serial Peripheral Interface (SPI) as master and slave. The slave interface as well as the HF interface can be used to transfer proper firmware onto the chip. The SPI master interface is used for communication with the transceiver. The sensor interface provides a temperature sensor which is used in this application and can be read out in software.
A firmware for the controller was already available, which provides functionality for the ASIG itself including HF communication and the SPI interface. The software was extended to get control of the transceiver chip and achieve the favored functionality of the sensor node. After starting up the node by connecting a power source, the firmware is started and automatically configuring the UHF transceiver and the HF interface. After that the HF interface can be used for additional modifications to the system configuration. If the configuration is done correctly, the transceiver enters sleep mode, otherwise the configuration starts again. Now that the communication interfaces work properly, the preliminaries for wireless communication are met. To successfully connect to the control unit, the requirements for encrypted communication have to be fulfilled first. Therefore, the key exchange procedure like presented in Figure 1.2, has to be accomplished by pairing the HF interface with the control unit. After these configurations are done, the sensor node is operational. By default the wireless sensor node operates in a low power mode to save energy. It only responds to the control unit if it receives any incoming request. If data is received on the UHF band, the transceiver wakes up and the controller collects and evaluates it. Typically, the data includes a message requesting temperature data from the control unit. The controller now reads the wanted sensor data from the corresponding register, sends it back to the transceiver which passes it on to the control unit. Thereafter, the transceiver falls back in sleep mode, waiting for another incoming transmission.
The sensor node is implemented in two different technologies, a highly miniaturized eWLB integration and a PCB version. A big advantage of the PCB version is the improved accessibility and more possibilities during testing. The structural design is nearly the same in both approaches (Figure 4.1).
The different parts of the wireless sensor node are described in detail in the following sections.

4.2 Onboard communication

To provide communication between the controller and the transceiver the synchronous Serial Peripheral Interface (SPI) bus is used. The controller (ASIG) acts as master and the transceiver (TDA5340) as slave. In order to communicate properly the interface of the controller has to be configured [12]:

- Most significant bit (MSB) first
- Chip Select (NCS) active low
- Clock polarity (CPOL) HIGH
- CPHA LOW
- baud rate about $100000 bit/s$

The SPI bus consists of 4 lines, Clock (SCLK), Chip Select (NCS), Master in Slave out (MISO) and Master out Slave in (MOSI). For communication with the transceiver, mainly three commands are used.

- Write Register
- Write TX FIFO
- Read RX FIFO

To configure the registers of the transceiver, the chip select line has to be low. Thereafter, an instruction byte and the address byte, followed by the data to write is sent. To end the write process, the chip select line goes high again [12].
To write the transmit FIFO (TX FIFO) the chip select line has to be activated. After sending the instruction byte, the next byte contains the number of data items minus 1 to be transferred into the FIFO. The following data bytes are stored into the FIFO. Only the number of bytes specified are stored. After completing the write operation, the chip select line is deactivated [12].
Reading from the receive FIFO (RX FIFO) first the chip select line is activated. Then the instruction byte must be sent. The transponder responds onto the command by shifting four bytes onto the bus; the following byte is a status word which contains the number of valid bits in the data packet. After completing the read operation, the chip select line is deactivated [12].

The TDA5340 provides interrupt lines which can be configured to become HIGH if any data is received from the UHF interface. Because the ASIG is not yet providing IRQ inputs, this lines cannot be used. Therefore, the controller is polling the input registers of the transceiver if some data has arrived. This is an adequate solution because the receiving FIFO of the TDA5340 can buffer 288 bits of data; big enough for no data getting lost.

4.3 HF Interface

Beside acting as the controller of the node, the ASIG also provides the HF communication interface. The interface is working with NFC compatible protocols. The antenna connected to the HF interface is implemented as a resonating coil operating at 13.56 MHz. This type of antenna is not used for transmitting electromagnetic waves; the communication distance is very small an therefore called near-field communication. The antenna is magnetically coupled with another coil in a HF reader or a smart phone as shown in Figure 4.2. As this antenna is highly inductive, some space for a capacitor must be spared on the PCB for realizing a matching to the exact frequency .

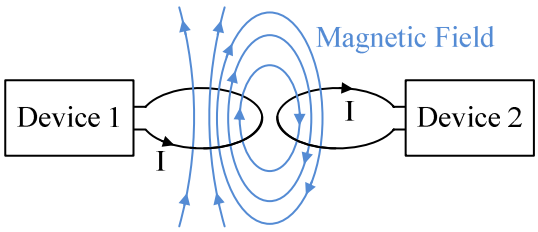

Figure 4.2: Near field magnetic coupling of two wireless devices

The HF interface can be used for programming and configuring the controller. For testing it is also possible to send commands across the chip directly onto the SPI bus.

4.4 UHF Interface

In general, the UHF interface consists of the above mentioned transceiver chip which is connected to a miniaturized UHF antenna. The TDA5340 is a multi-channel-multi-protocol transceiver developed by Infineon. The transmitter works as class-E RF amplifier configured for the 868 MHz UHF frequency band. A RF matching network combines the antenna matching, the external circuitry of the amplifier and the network for the receiving input. At the end of the matching network, a highly miniaturized UHF antenna designed for a resonant frequency of 868 MHz is connected. In addition to the matching network, the transceiver needs some passive elements to grant stable power supply [13].
The transceiver also needs to be configured by the controller before it works properly. After booting the node by connecting it to power supply, configuration of the transceiver is started. Therefore, several special function registers in the transceiver chip have to be set [12]. If this is successfully accomplished, the transceiver goes to sleep mode and only wakes up by a controller command or an incoming transmission. The transceiver has two separated FIFOs for receive and transmit, so it is buffering data if a collision in terms of timing occurs [12].

The used protocol for sending and receiving in this implementation is the simple 2kbit FSK EU Pattern [14]. The protocol was primarily used for testing the system. It can easily be changed by modifying the configuration.

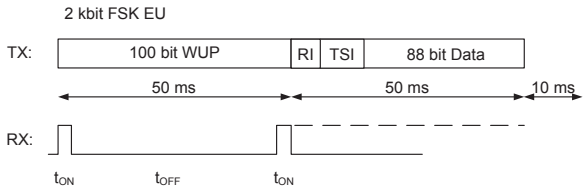

Figure 4.3: UHF protocol; 2kbit FSK EU pattern

Chapter 5

Antenna Design and Simulations

As mentioned in the last section, an eWLB and a PCB based implementation of the sensor node are considered. For both, the variety of possible UHF antenna designs is restricted by different properties of the corresponding realization. Each of the two technologies have a flat surface with little height, so planar antennas with low profile are preferred. In addition, the required area should be minimized. So, preferable types of antennas are the ones, which are small in terms of the wavelength at the center frequency. To meet the stated requirements, the inverted F antenna, the quarterwave monopole and the resonating loop antenna were investigated in further detail.

5.1 eWLB Antenna Design

The greatest challenge in the antenna design for the eWLB integration is doubtlessly the available space. The maximum side length for an eWLB package is 10 mm, resulting in an area of 1 cm^2. This area has to provide space for the antenna and the chip dies with their interconnections. Additionally, possible interactions between the chip dies and the metal connections in the package and the antenna have to be taken into account. For this reason, the sections for the antenna and the circuitry have to be well defined and must not overlap. The resulting partitioning of the eWLB package can be seen in Figure 5.1.

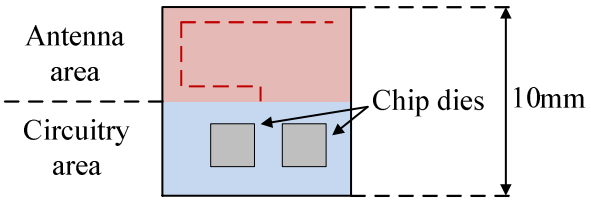

Figure 5.1: Partition of the eWLB

To perform an exact simulation of the antennas, a proper model for the substrate of the

eWLB has to be defined. In Figure 5.2 the substrate model shows the dielectric and metal layers as well as possible interconnections between them. The green layers represent the ASIG and the transceiver (TRX) and are included to be taken into account during the simulation. It was decided, to place the prototype of the eWLB on a PCB to make power supply easier. This PCB consists of a FR4 substrate with double-sided metal planes.

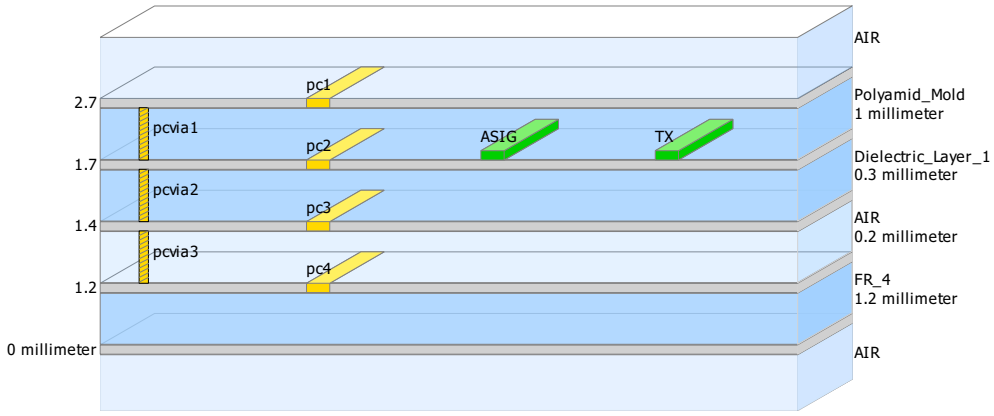

Figure 5.2: Substrate model of the eWLB package

5.1.1 Inverted F Antenna

As mentioned in Section 2.3.2, the advantage of the inverted F antenna is the possible avoidance of an additional matching network, achieved by a suitable antenna design. Since the size is a critical parameter for the discussed application, the focus lies on a good matching of the antennas. The precondition for achieving this benefit is an exact simulation.
The antenna is positioned on the pc2 layer shown in the substrate model of the eWLB (Figure 5.2).

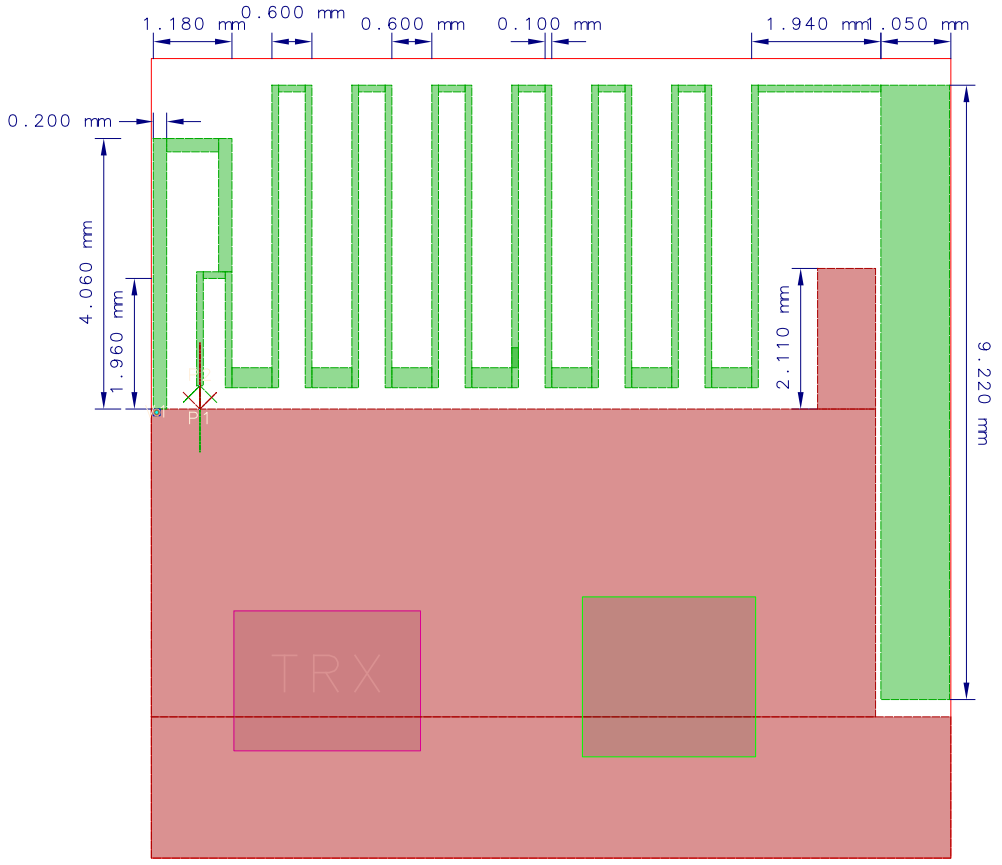

Figure 5.3: Design of inverted F antenna for the eWLB

The antenna design was designed iteratively starting with a typically inverted F antenna (see Chapter 2.3.2) and reducing the size step by step. The resulting design is presented in Figure 5.3.

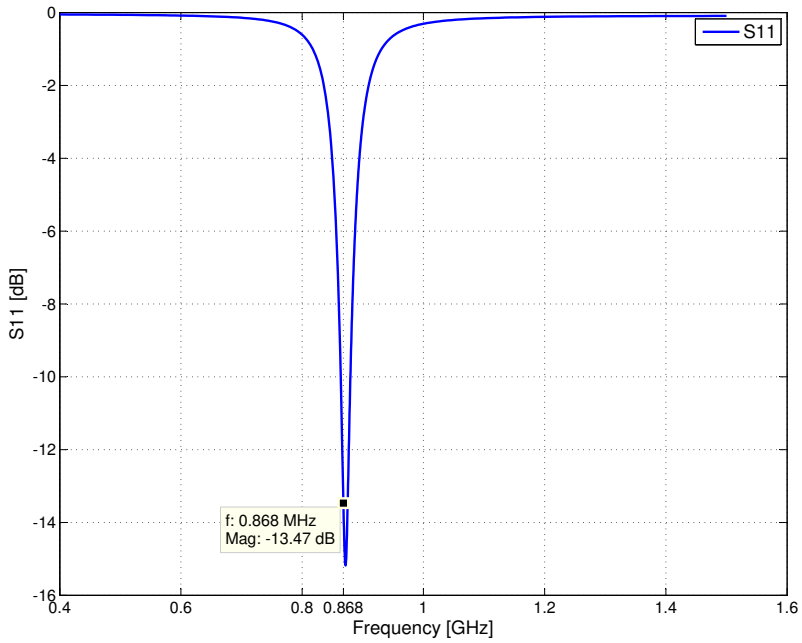

Figure 5.4: Simulated S11 parameter of the inverted F antenna for the eWLB

The simulations of the reflection coefficient and antenna impedance of the antenna are accomplished using a characteristic impedance $Z_0 = 50\,\Omega$. Figure 5.4 depicts the simulated reflection coefficient of the inverted F antenna. It can be seen that the antenna shows a good matching $\Gamma = -13.47\,\text{dB}$ at its center frequency. The bandwidth at which a $\Gamma < -10\,\text{dB}$ is accomplished is about 15 MHz around the center frequency of 872 MHz.

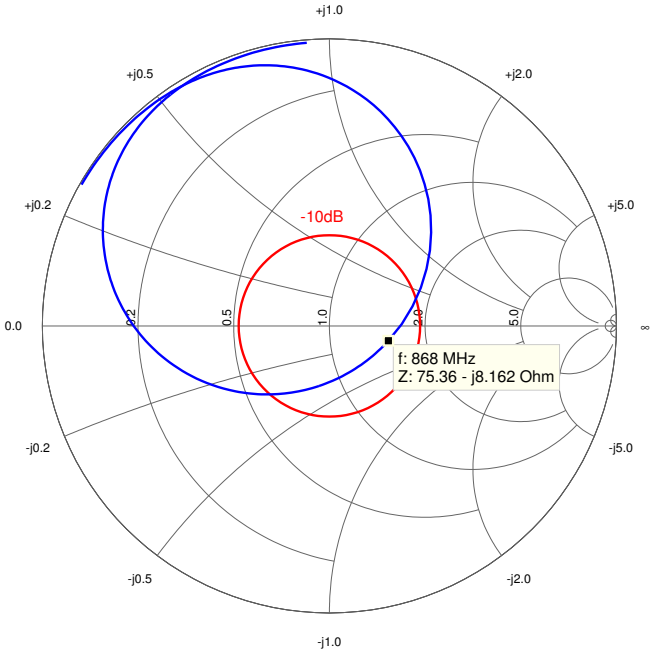

Figure 5.5: Smith chart for the inverted F antenna for the eWLB

In Figure 5.5 the Smith Chart shows the frequency response of the antenna impedance. At lower frequencies the antenna is highly inductive, becoming capacitive at the resonance frequency and showing a inductive impedance at higher frequencies again. The red circle illustrates the region, where the reflection coefficient is below -10 dB. The antenna impedance at 868 MHz is therefore indicated inside the red circle at $Z = 75.36 - j8.16\,\Omega$.

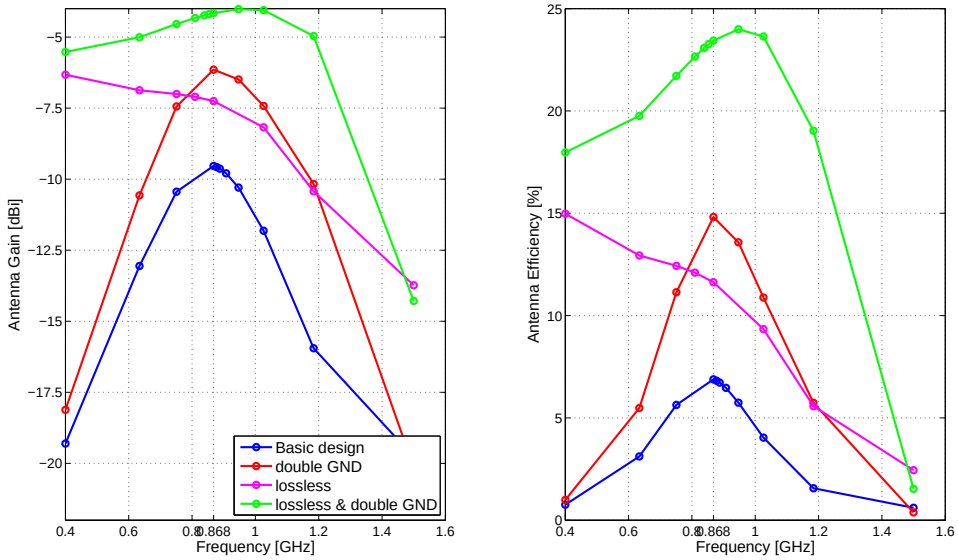

Figure 5.6: Simulation results of the antenna gain and efficiency of the eWLB inverted F antenna at different conditions

The parameters, such as antenna gain and efficiency, indicate the antennas radiation performance; these parameters are shown in Figure 5.6. The antenna simulation was performed for loss-less (red line) and real (blue line) materials combined with increased ground planes (magenta and green line). It turns out that the antenna is optimized for the considered frequency band at 868 MHz. The simulation shows that losses dependent to the material have great influence on the antennas performance. On the other hand the limited antenna area and small ground plane available on the eWLB highly reduces efficiency and antenna gain as well. The results of the simulation for the antenna efficiency and gain are summarized in Table 5.1.

eWLB IFA	Gain [dBi]	Efficiency [%]
Basic design	-9.53	7
Doubled ground plane	-6.15	15
Lossless	-7.25	12
Lossless with doubled ground plane	-4.16	24

Table 5.1: Gain and efficiency of the eWLB inverted F antenna at 868 MHz; at different simulation conditions

5.1.2 Loop Antenna

The loop antenna is introduced more detailed in Chapter 2.3.2. The design is carried out on the layers PC2 and PC3 of the eWLB; (compare Figure 5.2). The two-layer approach gives an advantage for designing the capacitor, needed for gaining resonance. It gives the possibility to overlap the capacitor plates using the substrate of the circuit board as the dielectric medium, and therefore, increase the capacitance. The resulting antenna design is presented in Figure 5.7.

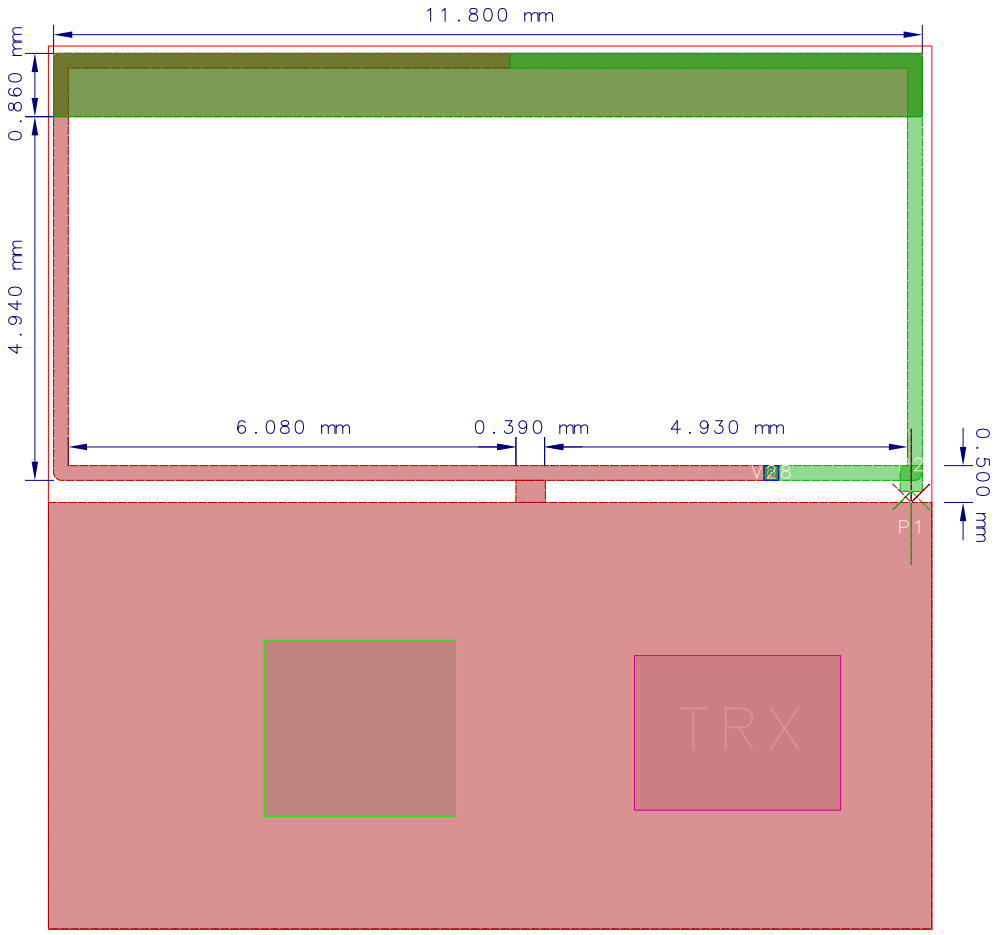

Figure 5.7: Design of the loop antenna for the eWLB

The results of the S-Parameter simulation are plotted in Figure 5.8. As can be seen, the reflection coefficient at 868 MHz is -20.91 dB, which means less than 1 % of the power transmitted to the antenna, is reflected. The simulation predicts a reflection coefficient not higher than -10 dB from 857 MHz to 875 MHz resulting in a bandwidth of 18 MHz at a center frequency of 866 MHz.

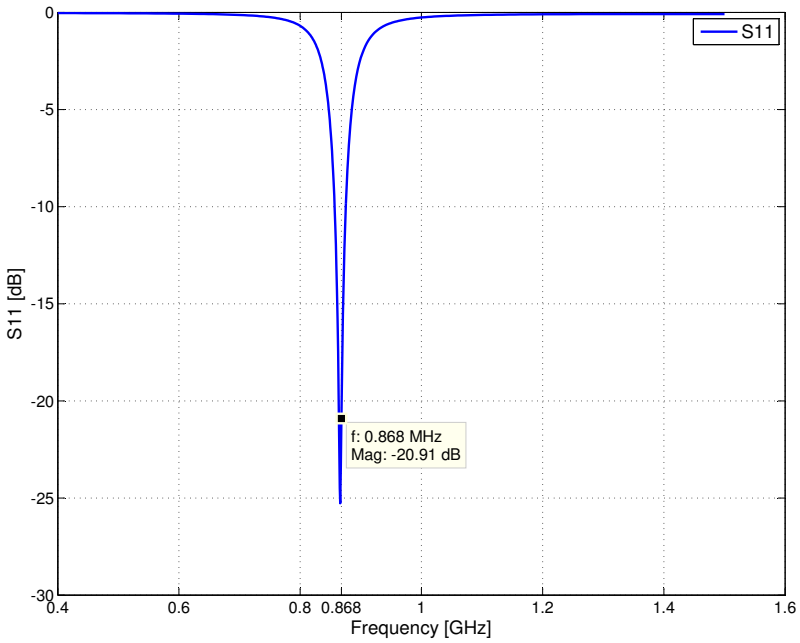

Figure 5.8: Simulated S11 parameter of the loop antenna for the eWLB

The good results for the reflection coefficient also implies acceptable feeding impedance for this antenna. The Smith Chart (Figure 5.9) shows that eWLB loop antenna is nearly resonant at 868 MHz. At this frequency the antenna impedance crosses the horizontal axis of the Smith Chart, which indicates the imaginary part of the antenna impedance is zero. It can be seen, that the antenna is inductive before reaching their resonant frequency and gets capacitive for a short frequency interval before getting inductive again.

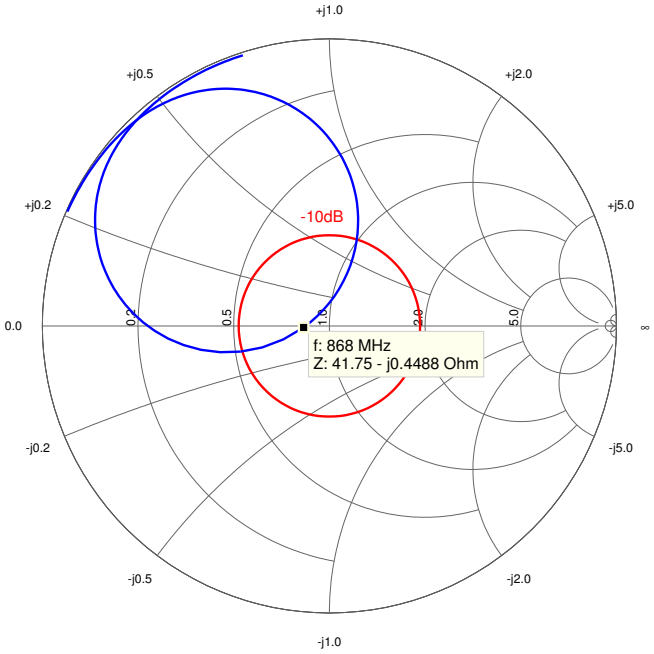

Figure 5.9: Smith chart for the loop antenna for the eWLB

The simulations of the antenna gain and efficiency of this antenna was also performed under different conditions, as described in Subsection 5.1.1. The simulation results presented in Figure 5.10 obviously show the bad performance of the loop antenna. It was expected that the efficiency of this antenna is below average, because this type of antenna suffers very much from reduced antenna size, but the actual result unfortunately turned out to be worse. The simulation studies with different materials and increased ground plane size do not have much influence on the performance of the antenna. Still, as mentioned in Section 2.3.2 the antenna has been analyzed because of the matching benefits. However, the graph shows that the performance of the antenna rapidly increases at higher frequencies. It suggests that this antenna in the required size is not suitable for the required frequency.

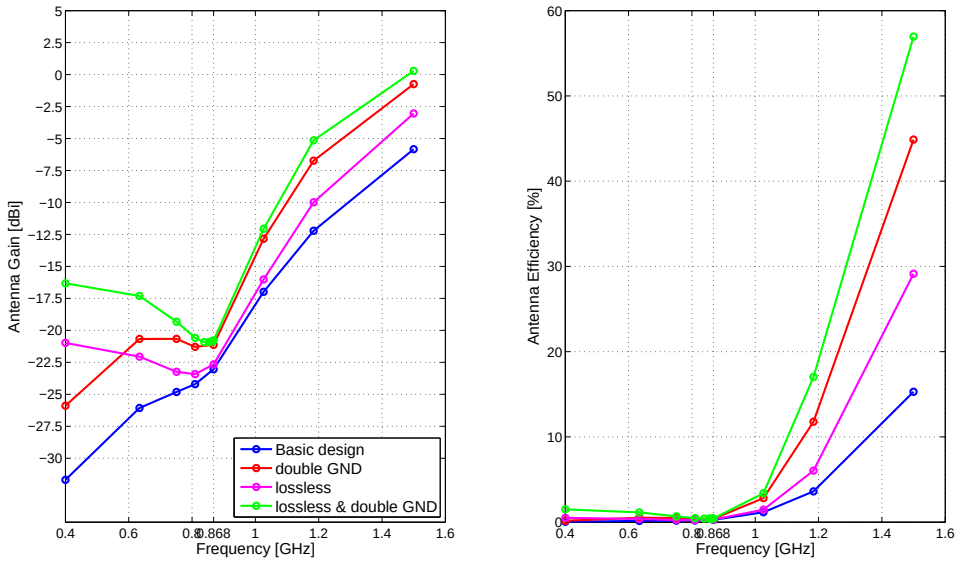

Figure 5.10: Simulation results of the antenna gain and efficiency of the eWLB loop antenna at different conditions

5.2 Design for direct Integration on a Printed Circuit Board

The second approach for the sensor node is the integration of the whole system on a printed circuit board. The different antennas have to be realized on the PCB as well. The different dielectric coefficient of the substrate requires a adapted antenna design. First an estimation of the circuit layout was performed to find out how much space is available (Chapter 6.2). Figure 5.11 shows the resulted partitioning of the PCB. Positioning the whole circuit layout on the top layer and the ground plane on the bottom would be the optimal solution. Because of particularities of the ASIG design, the limitations for an efficient PCB layout were imposed.

The area on the printed circuit board reserved for the antenna is approximately $27 \times 10\,\mathrm{mm}^2$ which is more than the one available on the eWLB based design. Hence, the antennas designed for the eWLB need to be adapted or newly designed for proper function on the PCB.

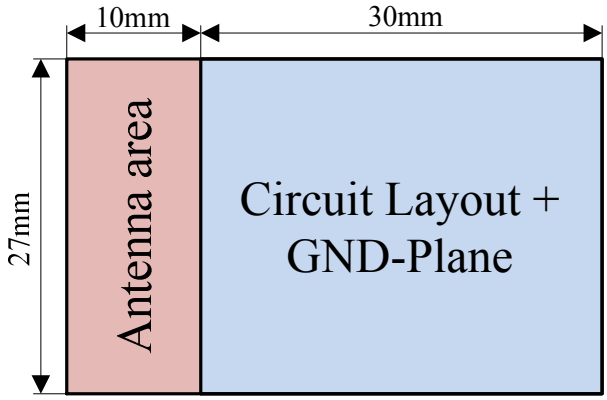

Figure 5.11: Partition of the printed circuit board

For the system implemented on a printed circuit board, three different antenna types are be designed:

- Inverted F antenna (IFA)
- Loop antenna
- $\lambda/4$ monopole

For the implementation of the PCB, a double layer FR4 substrate was selected. The corresponding substrate model for the simulation can is presented in Figure 5.12.

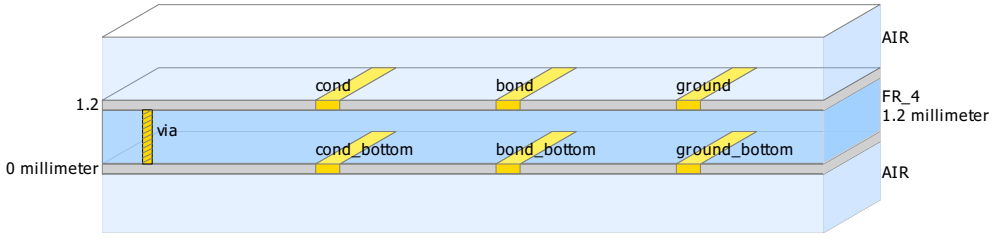

Figure 5.12: Substrate model of the printed circuit board

The relative permittivity of FR4 is usually between $\epsilon_r = 4.3$ to $\epsilon_r = 4.8$ [15] [16]. The manufacturer of the printed circuit board gives a value of $\epsilon_r = 4.6$ [17] which is very high. Substituting this into (2.33) the resulting wavelength in the substrate is about $\lambda_s = 161\,\text{mm}$ at 868 MHz. Due to of the surrounding air, the effective permittivity (2.34) results to $\epsilon_{\text{r,eff}} = 3.2$.

Frequency [MHz]	λ_0 [mm]	λ_{eff} [mm]	$\lambda_{\text{eff}}/4$ [mm]
868	345.6	193.2	48.3

Table 5.2: Wavelength for FR4-PCB h=1.2 mm, $\epsilon_r = 4.6$, $\epsilon_{\text{r,eff}} = 3.2$

5.2.1 Inverted F Antenna

The optimal design is similar to the one described in Chapter 2.3.2. For the new IFA an existing design was adapted and minimized. Achieving this, the main radiator is a meandered line of 88 mm length and 0.2 mm width; ending in a 1 mm wide line of 18 mm length. The design was optimized during simulation and resulted in the final design in Figure 5.13. The grounded stub provides impedance adjustment for matching the antenna to the transmission line. Because the simulations did not consider the detailed circuit layout on the PCB, performance changes were predetermined. Therefore, placeholders for an additional matching network are provided in the circuit layout. Furthermore, a second IFA design (now called IFAv2) which is orientated in the opposite direction was realized (Figure 5.14).

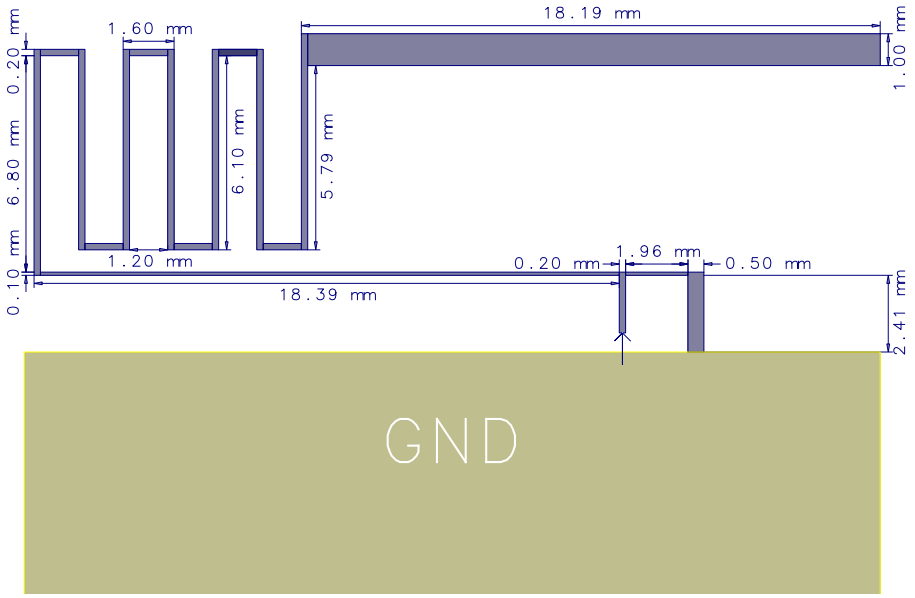

Figure 5.13: Design of inverted F antenna v1

There are only little differences between the two designs reasoning a fixed position of the feed point. The main radiator of IFAv2 is increased by 15 mm compared to IFAv1.

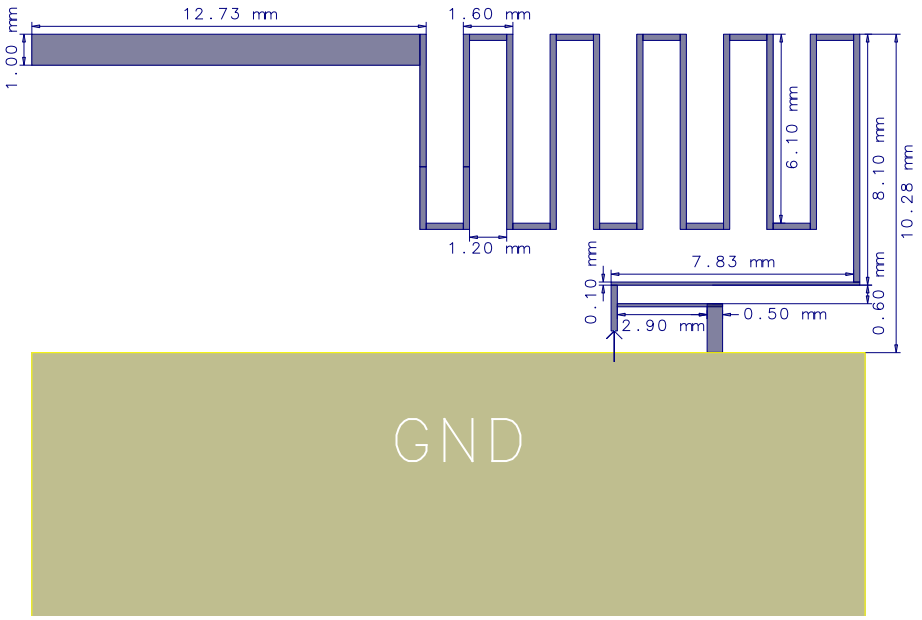

Figure 5.14: Design of inverted F antenna v2

The EM-simulation of these two antennas visualizes how the current is distributed on the radiation element. In Figure 5.15 and Figure 5.16 the color of the arrows indicate the current density on these two antennas. Because inverted F antennas are quarterwave antennas, the standing waves of current and voltage feature only one maximum at different positions. As required, the current wave has its maximum at the feed point and decreases along the antenna.

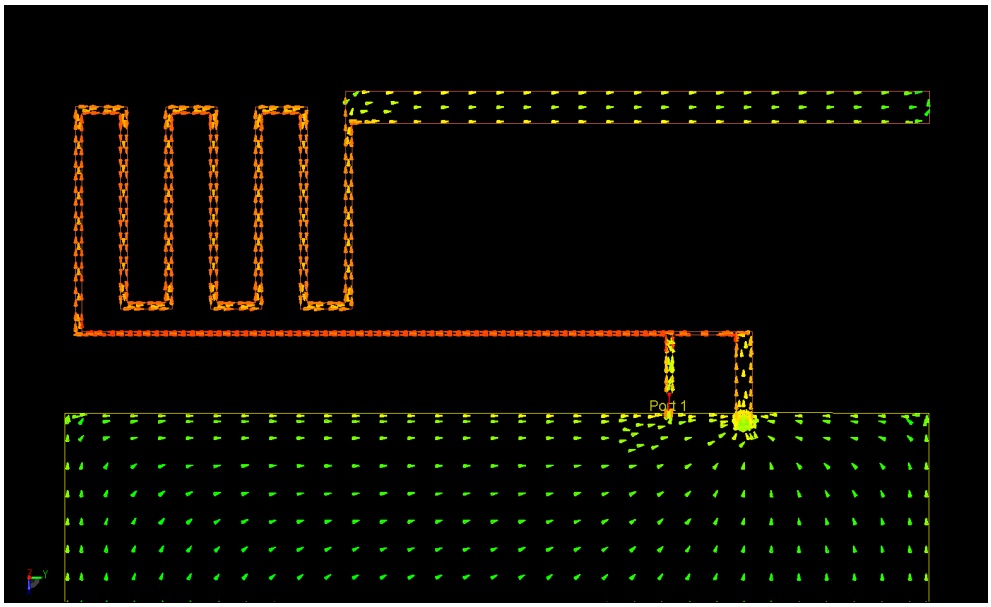

Figure 5.15: Current distribution of the Inverted F antenna type 1

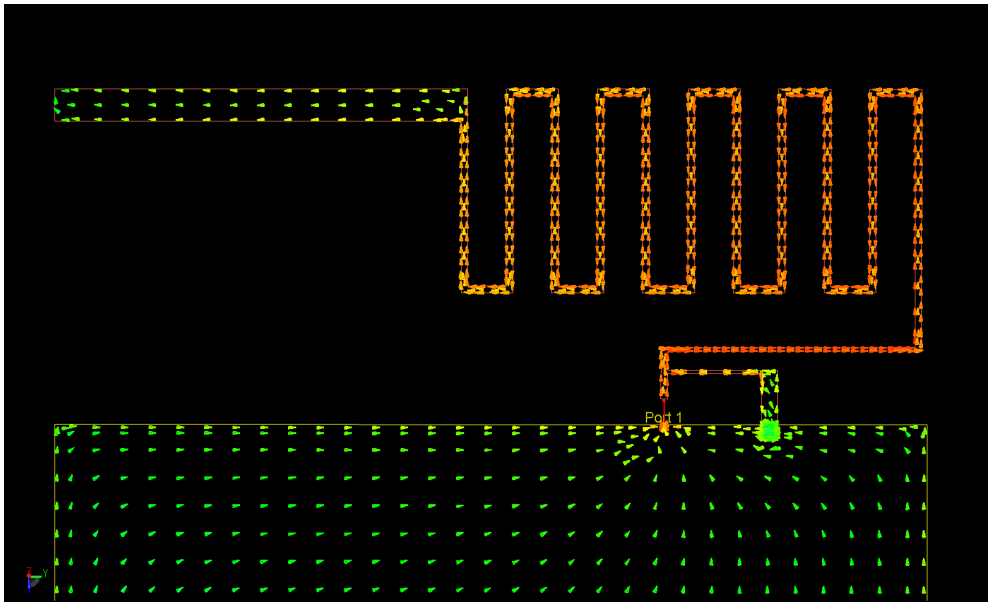

Figure 5.16: Current distribution of the Inverted F antenna type 2

Furthermore some antenna parameters are needed to give information about the antenna performance.
The S-parameter simulation results are depicted in Figure 5.17. The reflection coefficient of antenna IFAv1 and IFAv2, respectively, is represented by the blue curve and the green curve. As presented in the diagram, matching of antenna one with $\Gamma_{\mathrm{IFAv1}} = -17.46\,\mathrm{dB}$

is slightly better than $\Gamma_{\mathrm{IFAv2}} = -13.12\,\mathrm{dB}$ of antenna 2. The bandwidth over which the reflection coefficient is below $-10\,\mathrm{dB}$, is about 11.4 MHz for antenna 1 and 12.5 MHz for antenna 2.

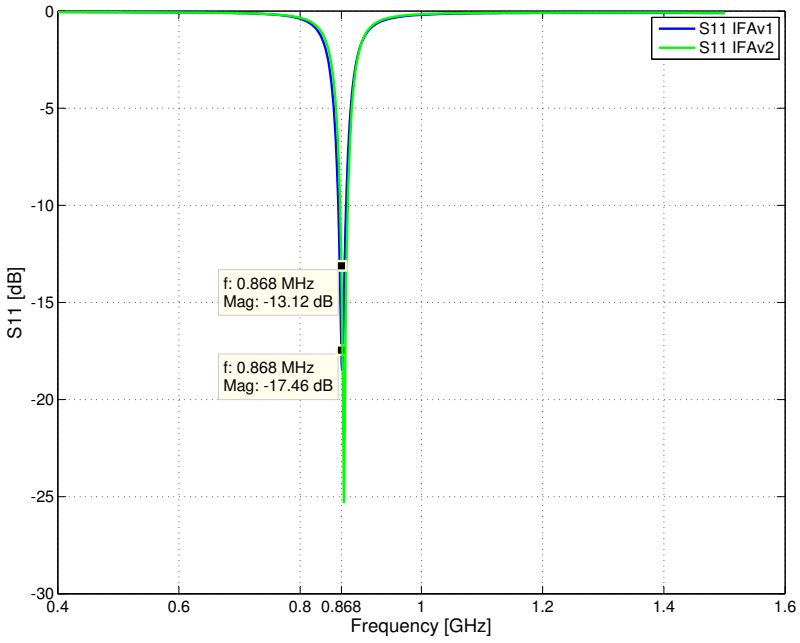

Figure 5.17: Simulated S11 parameter of both inverted F antennas

The good results for the reflection coefficients also imply acceptable feeding impedance for these two antennas. The Smith Chart (Figure 5.18) shows that both are nearly resonant at 868 MHz. The antenna is at resonance where the impedance line crosses the horizontal axis, which indicates the imaginary part of the antenna impedance is zero. It can be seen, that the antennas are inductive before reaching their resonant frequency and get capacitive when rising beyond it. Moreover, the resistive part of the antenna impedance is about $62\,\Omega$ for IFAv1 and $70\,\Omega$ for IFAv2, which is in a range where matching to a $50\,\Omega$ transmission line should easily be possible. The area within the red circle illustrates the region, where the reflection coefficient is below -10 dB.

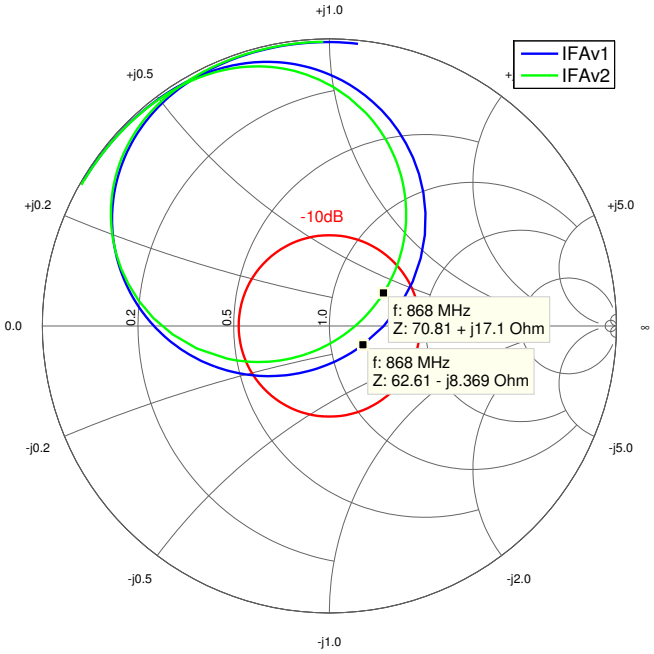

Figure 5.18: Smith diagram of both inverted F antennas

Two essential parameters for radiation characteristics, antenna gain and efficiency, are plotted in Figure 5.19, for antenna IFAv1, and in Figure 5.20, for IFAv2. The blue graphs in the diagrams indicate the performances of the final antennas. Though the simulation results for the antenna efficiency present a maximum of 37 % in the desired frequency band between 860 MHz and 900 MHz, the performance of the antennas is not very good. These losses of antenna gain and efficiency were expected, because of the small antenna size and ground plane. Additional simulations with an increased ground plane and lossless materials highlighting this relationship. It turned out, that an increasing the ground plane by factor two, gives an efficiency boost of 20 % and the losses of the materials are responsible for another 20 %. As expected, this lack in performance is the result of the trade-off between efficiency and size. A comparison of the different simulation results are summarized in Table 5.3.

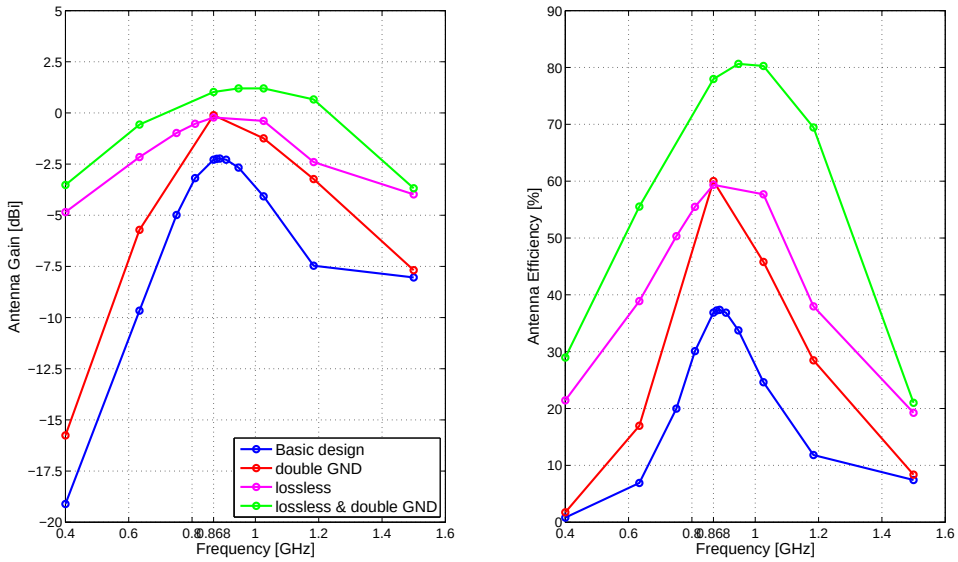

Figure 5.19: Simulation results of the antenna gain and efficiency of IFAv1 at different conditions

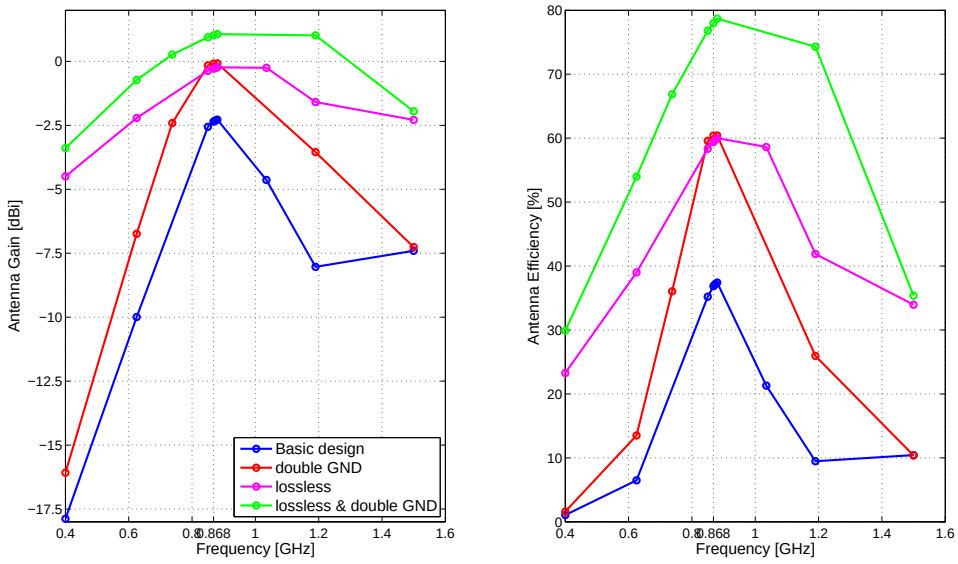

Figure 5.20: Simulation results of the antenna gain and efficiency of IFAv2 at different conditions

	Gain [dBi]		Efficiency [%]	
Antenna	IFAv1	IFAv2	IFAv1	IFAv2
Basic design	-2.29	-2.35	37	37
Doubled ground plane	-0.11	-0.09	60	60
Lossless	-0.22	-0.28	60	59
Lossless with doubled ground plane	1.02	1.02	78	78

Table 5.3: Gain and Efficiency of both Inverted F antennas at 868 MHz; at different simulation conditions

5.2.2 Loop Antenna

The loop antenna was introduced in detail in Chapter 2.3.2. The design covers both layers of the PCB. This gives some advantages in achieving the capacitance, needed to gain resonance. It gives the possibility to overlap the capacitor plates using the substrate of the circuit board as the dielectric medium, and therefore, increase the capacitance.

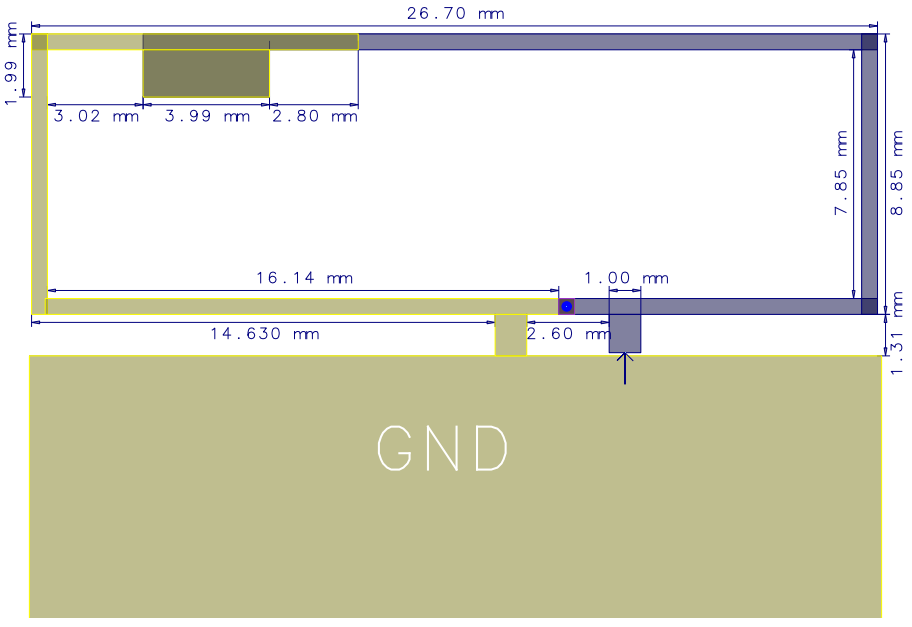

Figure 5.21: Design of the loop antenna

Because of expected differences between the simulated and the final antenna, the design of the capacitor plates allows subsequent minimal modifications on the PCB. In this way it is possible to vary their size for better matching and perhaps avoiding a matching network completely. As a precaution, the slots for external matching components are still available on the PCB. The length of the grounded stub between the feed and ground line was investigated during simulation and fixed at a length of 2.6 mm as shown in Figure 5.21. Both, feed and grounded stub are 1 mm wide. The main radiator is a 71.1 mm bent line,

with side lengths of 26.7 mm and 8.85 mm.

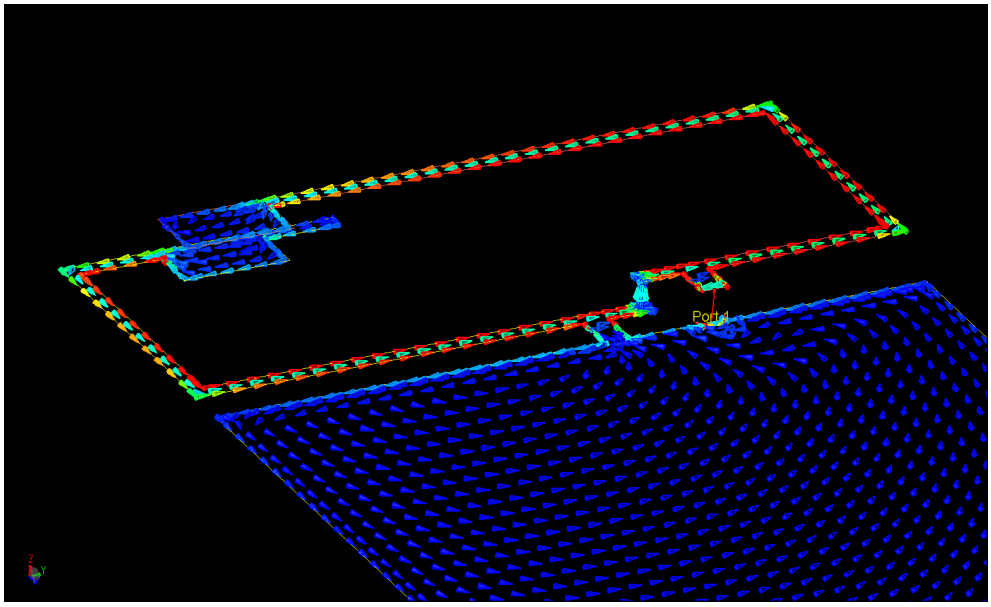

Figure 5.22: Current distribution of the loop antenna

As seen in Figure 5.22, the current distribution is nearly constant over the antenna.

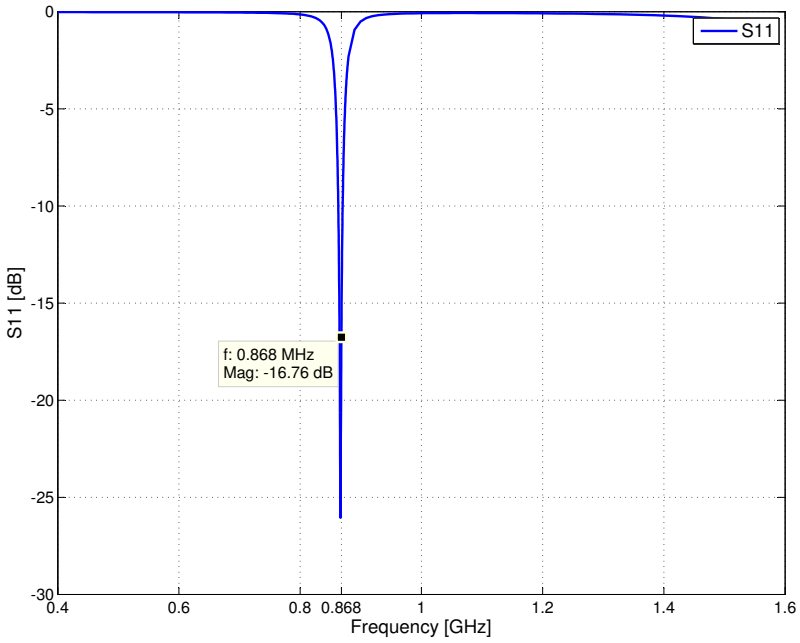

Figure 5.23: Simulation of S11 parameter of the loop antenna

The results of the S-Parameter simulation are plotted in Figure 5.23. As can be seen, the

reflection coefficient at 868 MHz is -16.76 dB, which means not more than 2 % of the power transmitted to the antenna, is reflected. The simulation predicts a reflection coefficient not higher than -10 dB from 863 MHz to 870 MHz resulting in a bandwidth of 7 MHz.
The same data is displayed in the Smith Chart in Figure 5.24, showing that the antenna is inductive at lower frequencies and gets capacitive with increasing frequencies. It can be recognized, that the antenna is resonant near the center point in the Smith Chart with an impedance of $Z = 41.1 - j9.9\,\Omega$ at 868 MHz. Therefore, the antenna seems well matched to the characteristic impedance of the transmission line of $Z_0 = 50\,\Omega$.

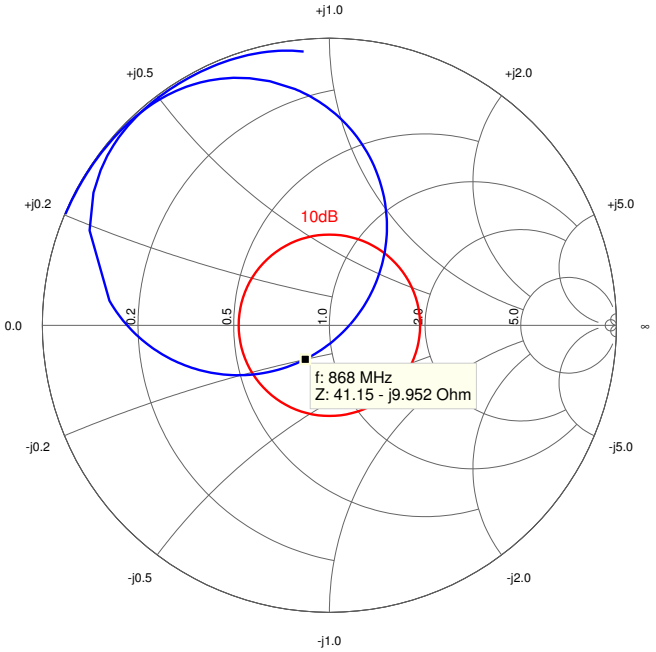

Figure 5.24: Smith diagram of the loop antenna

The antenna gain and efficiency presented in Figure 5.25 for the loop antenna are not very high. Such a behavior was expected as this type of antenna suffers very much from reduced antenna area. As mentioned in Section 2.3.2, the antenna was chosen because of the matching benefits. The graphs highlights that the performance of the antenna increases rapidly at higher frequencies, respectively, at shorter wavelengths. Also the simulation studies with different materials and increased ground plane size are not showing better results. The area and size of the radiating element itself is too small for this frequency. It turns out that this antenna is not the best choice, if area is a restriction for the design.

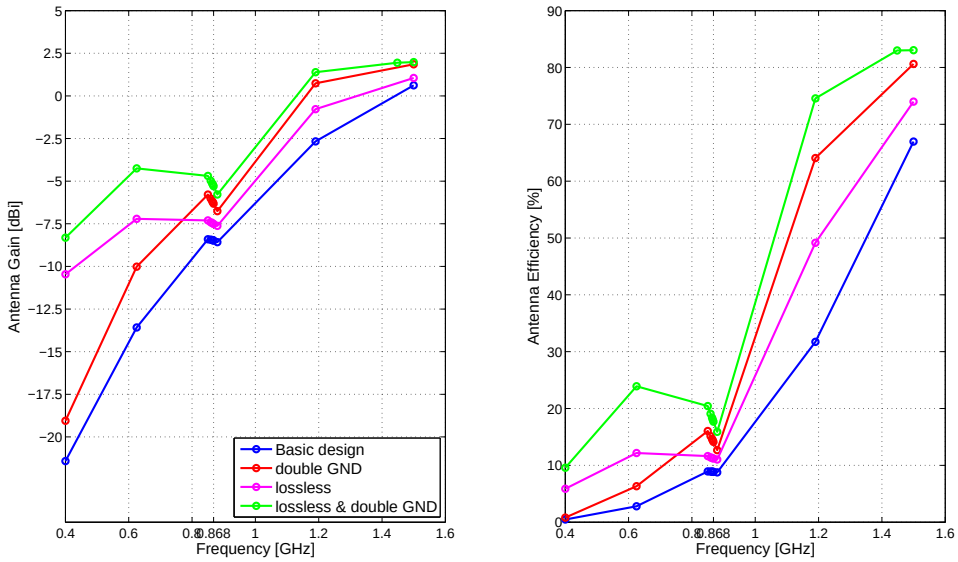

Figure 5.25: Simulation results of the antenna gain and efficiency of the Loop antenna at different conditions

Loop Antenna	Gain [dBi]	Efficiency [%]
Basic design	-8.48	9
Doubled ground plane	-6.32	14
Lossless	-7.51	11
Lossless with doubled ground plane	-5.30	18

Table 5.4: Gain and efficiency of the loop antenna at 868 MHz; at different simulation conditions

5.2.3 Monopole Antenna

Theory and functionality of a monopole antenna was discussed in Chapter 2.3.1. On the one hand, it was expected that the radiation efficiency for this antenna is slightly better than for the others. On the other hand, a proper matching network for the antenna is certainly needed. The designed antenna has a ground plane of 30x27 mm^2 and an effective area for the radiator of 10x27 mm^2. During simulation, the best design was derived empirically. The main radiator is a 99 mm meandered line which is 0.5 mm wide (Figure 5.26).

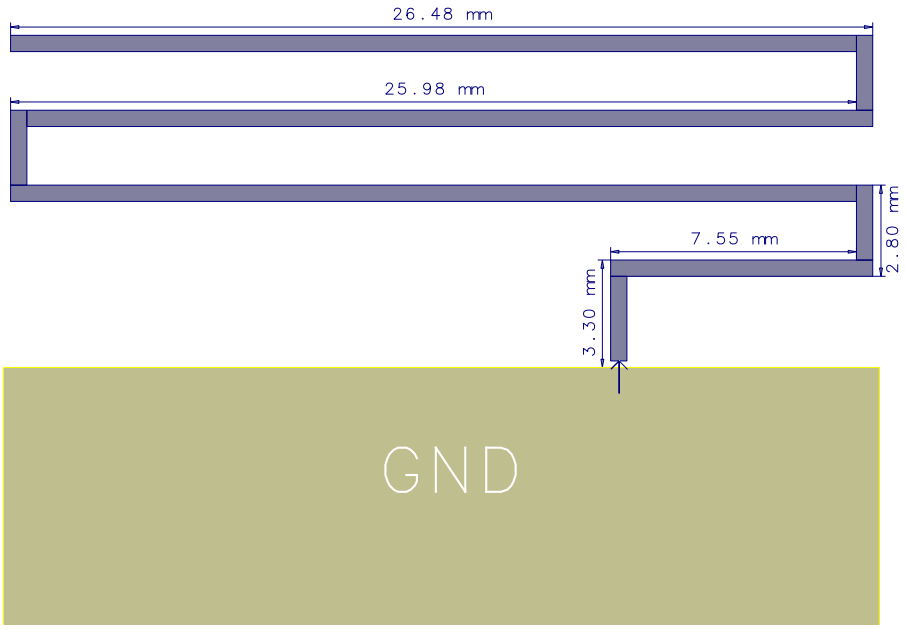

Figure 5.26: Design of monopole antenna

The current distribution in Figure 5.27 is rather good, but the current is not very high because the antenna is not resonant at 868MHz.

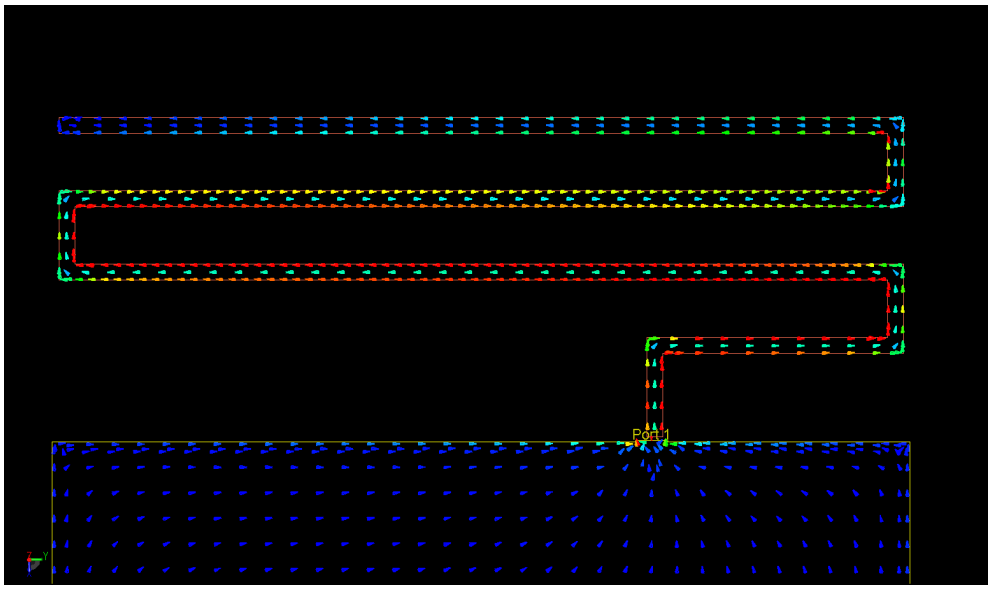

Figure 5.27: Current distribution of the monopole antenna

As highlighted in Figure 5.28 the antenna itself is resonant near 990 MHz. To get an acceptable reflection coefficient an additional matching network has to be realized on the PCB.

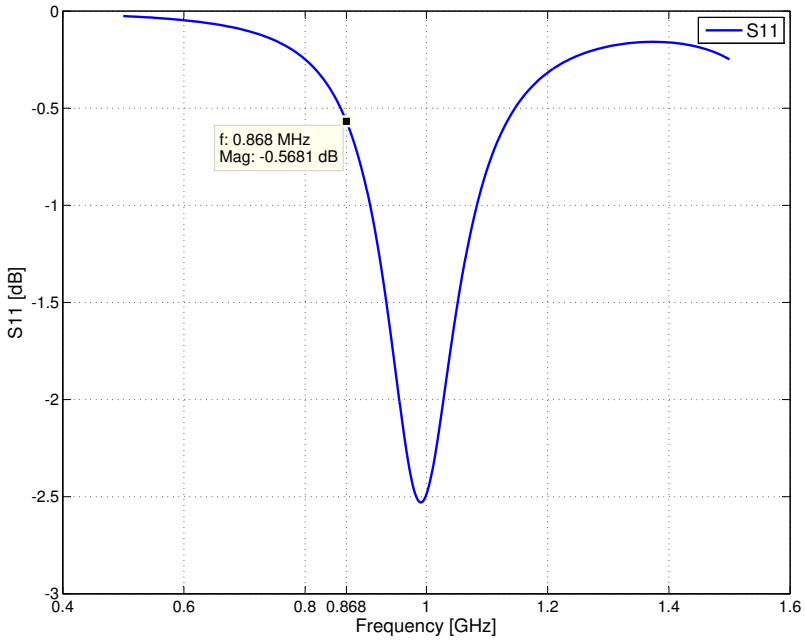

Figure 5.28: Monople S11 parameter with (blue) and without (red) loading coil

The Smith Chart in Figure 5.29 depicts the mismatching of the antenna very well.

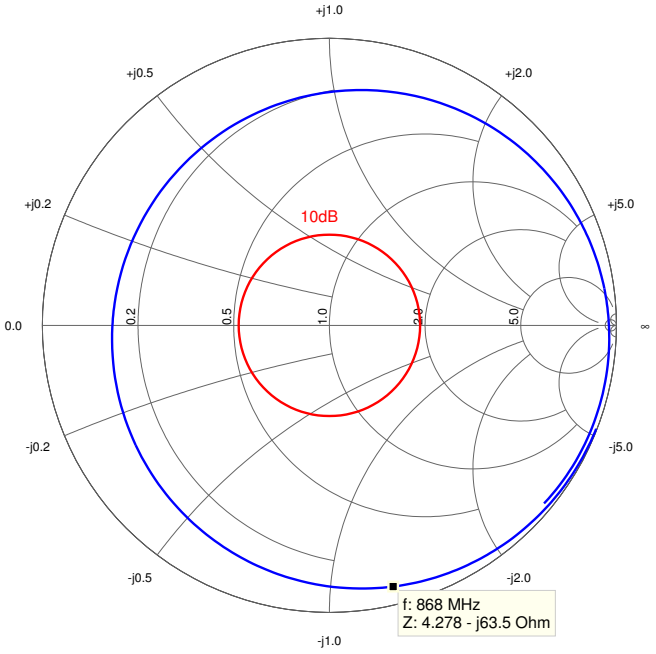

Figure 5.29: Smith diagram of the monopole antenna

Despite of the bad matching of this antenna, the monopole was investigated because of the efficiency and gain, which was expected to be better than at the other designs. The output of the EM simulation in Figure 5.30 demonstrates this quite well. The efficiency of the monopole, at the used frequency (868 MHz), of 55 % (Table 5.5) shows an increase of 20 % compared to the inverted F antennas. Without losses and an increased ground plane, theoretically an efficiency of 80 % can be reached with this antenna. Additional lack of performance results from the meander shape of the antenna, because the optimal design of a monopole antenna would consist of a straight radiator arranged perpendicular to a ground plane.

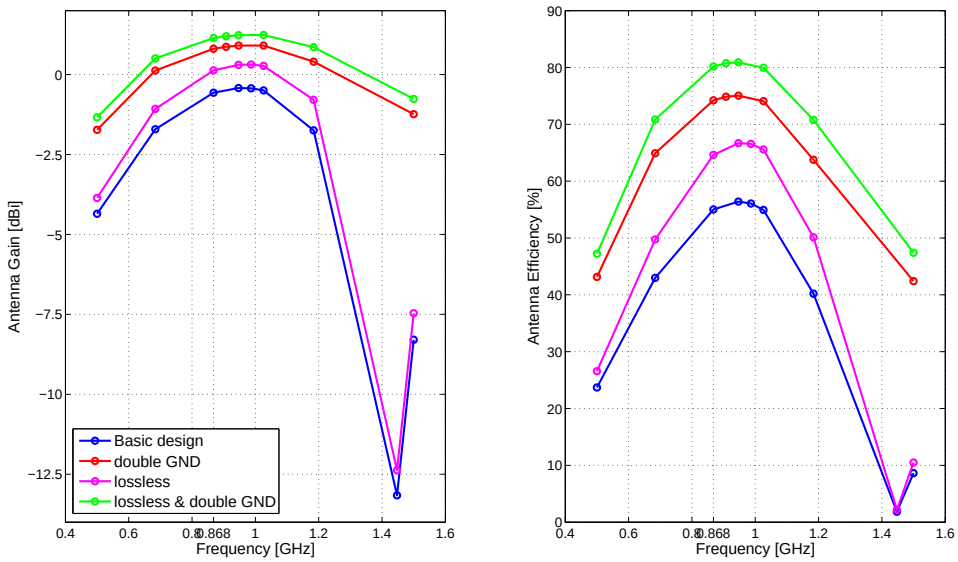

Figure 5.30: Simulation results of the antenna gain and efficiency of the Monopole antenna at different conditions

Monopole Antenna	Gain [dBi]	Efficiency [%]
Basic design	-0.57	55
Doubled ground plane	0.81	74
Lossless	0.13	65
Lossless with doubled ground plane	1.14	80

Table 5.5: Gain and Efficiency of the Monopole antenna at 868 MHz; at different simulation conditions

5.2.4 HF Antenna

The design for the HF antenna was adopted from an existing RFID Tag and reduced in size. The resonant coil shown in Figure 5.31 consists of 5 windings with a width of 0.5 mm and a spacing between the windings of 0.5 mm. The coil covers a space of 25.16 mm × 26.9 mm. The inductance of the HF coil is 993 nH and the resistance is 22.5 Ω.

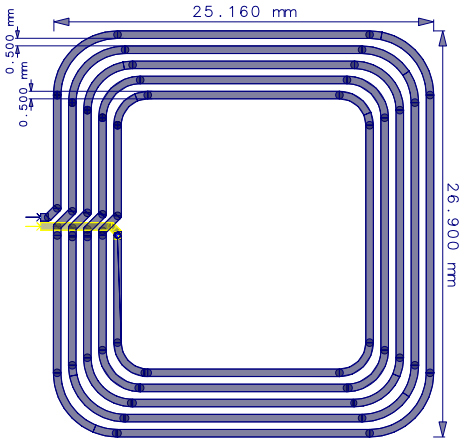

Figure 5.31: Design of HF antenna

As the HF antenna is not more than an inductance, the antenna has to be matched before any performance details can be evaluated. The simulation of the HF antenna was done by two steps. First the antenna layout was simulated using a EM simulator and an EM-model was generated. This model is used in a cosimulation to evaluate the required passives for a matching network. The simulation setup with the already dimensioned matching network is depicted in Figure 5.32. The matching network consists of one capacitor $C_1 = 110\,\text{pF}$ in parallel and one capacitor $C_2 = 29\,\text{pF}$ in series. The capacitor C_1 and the HF coil form a oscillating circuit and are in resonance at the frequency of 13.56 MHz (Figure 5.33). The resistor R_1 can be used to decrease the quality factor of the oscillating circuit thus increasing the bandwidth. As presented in Figure 5.33 the simulation results show a good performance for the selected matching network.

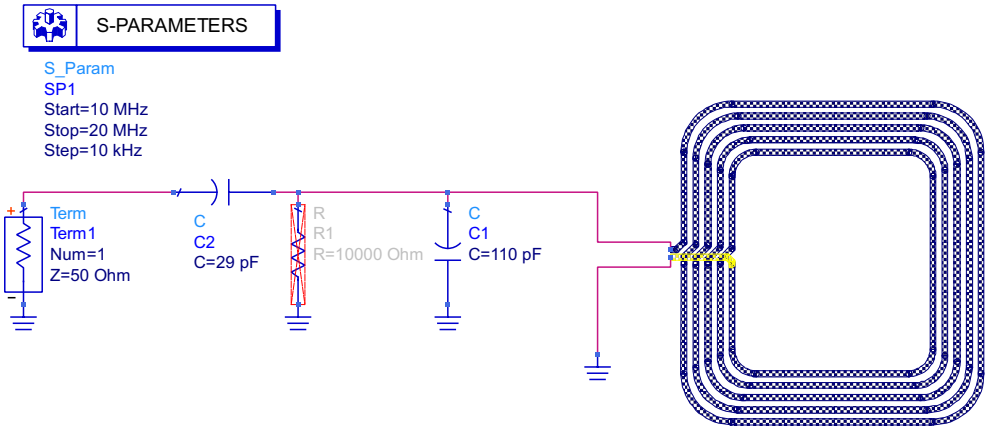

Figure 5.32: Simulation setup for the matching network of the HF antenna

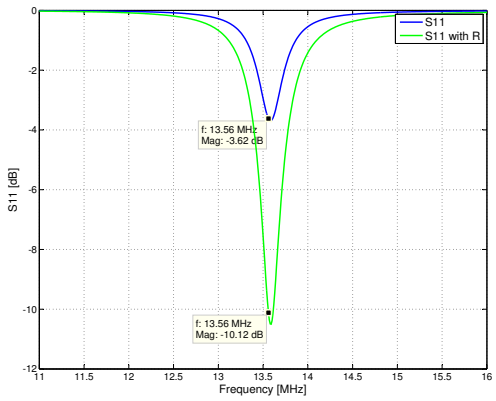

Figure 5.33: Simulation results of the S11 simulation of the HF antenna for two different matching networks

Chapter 6

System Design - Implementation

This chapter describes the implementation of the wireless sensor node. First, the design of the electric circuit is discussed in Section 6.1, followed by description of the layout of the printed circuit board in Section 6.2. The written firmware is elaborated in Section 6.3.

6.1 Circuit Design

Most of the circuitry for the wireless sensor node was adopted from the ”’Test Circuitry Evaluation Board”’ in the transceiver manual [13]. The circuitry mainly consists of the power supply, the circuitry for the class-E amplifier of the UHF transceiver, including the matching network for the antenna, and the SPI interconnection wires. To improve accessibility and testability, all SPI bus lines are wired to connectors.

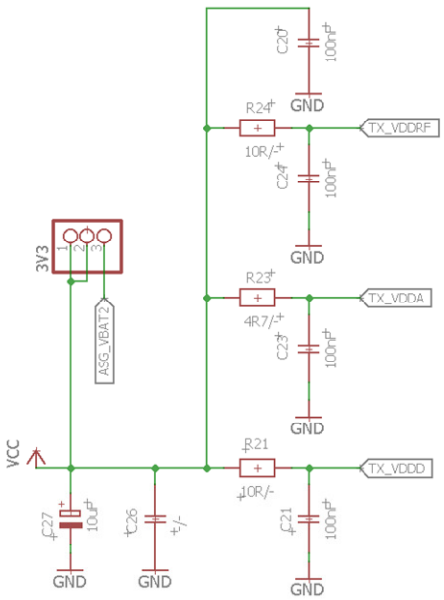

Figure 6.1: Power supply of the wireless sensor node

The wireless sensor node operates with a supply voltage of 3.3 V. To keep the power supply lines clean of voltage drops and high-frequency couplings, blocking capacitors are added to the power supply lines (Figure 6.1). The resistors at the individual supply pins of the TDA5340 grant the needed voltage levels for all internal parts of the transceiver [13].
Figure 6.2 depicts the matching network. The matching network consists of the circuitry for the class-E amplifier at the output of the transceiver, the input network of the transceiver and the matching network for the antenna. The values for the electrical components of the output and input network are configured for 868 MHz and taken from the transceiver manual [13]. All the electrical components for the matching network are high performance HF components, meeting the requirements for the used frequency band. For the antenna matching network, two slots ($C15$ and $C19$) are reserved in the layout.

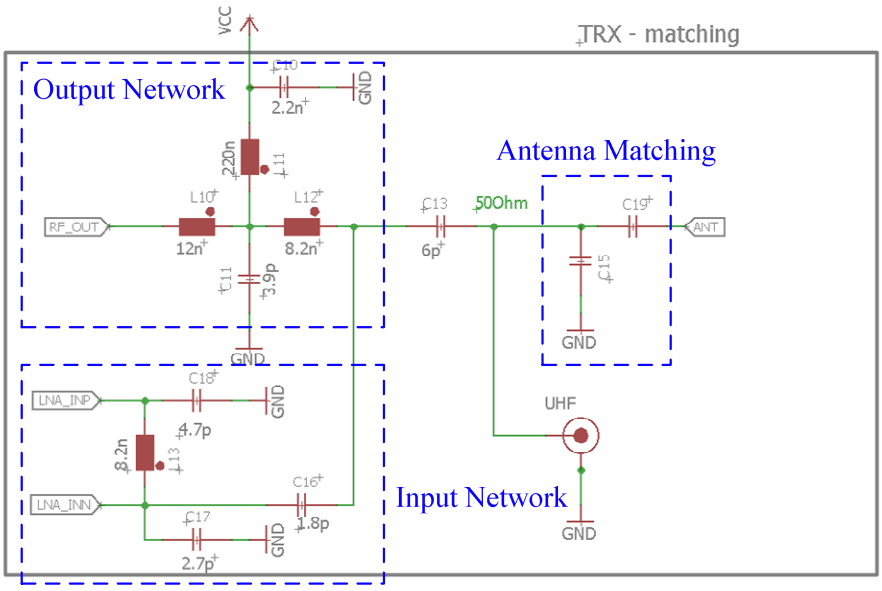

Figure 6.2: Matching network and external circuitry of the UHF transceiver

6.2 PCB for Chip-on-Board Design

The printed circuit board is designed as a double-layer board with FR4 substrate. The soldering layer is primarily used as a ground plane for the antenna and should not be intersected by other connections. Hence, all circuit components and interconnections are placed on the component layer of the board. All free space remaining between the connections is used as ground plane. Another point is, to consider that high frequency circuits and other connections, especially digital data lines, influence each other. To provide a proper function of the HF section on the board, all other connections, have to be separated from the HF transmission lines and the matching network. An additional arrangement to reduce disturbances, keeps the current flow on the ground plane constant.

To achieve this, the ground planes on both layers are interconnected by a high number of vias. Especially the matching network is caged in by a surrounding border consisting of interconnection between the two layers. For achieving higher miniaturization, the chip dies of the integrated circuit are bonded directly to the printed circuit board.

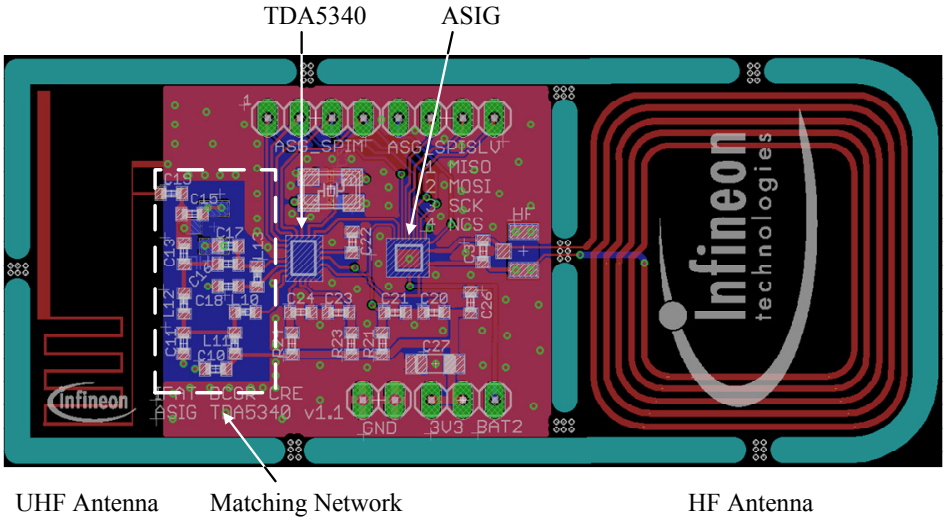

Figure 6.3: Printed circuit board layout of the wireless sensor node

Figure 6.3 depicts the layout of the printed circuit board. The UHF antenna is placed on the opposite end of the board than the HF antenna. This approach was realized, because the disturbances of the HF antenna have a great influence on the performance of the UHF antenna. To avoid this, the physical distance between these two antennas is maximized.

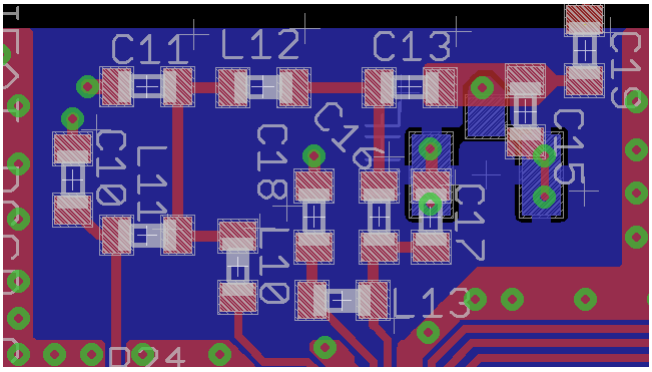

Figure 6.4: Detailed view of the matching network

Next to the UHF antenna, the matching network (see Figure 6.4) is placed, further con-

nected to the transceiver chip. The power supply is positioned on the lower edge of the printed circuit board with the additional power connector; and the the external connectors for the SPI bus lines are placed on the upper edge.

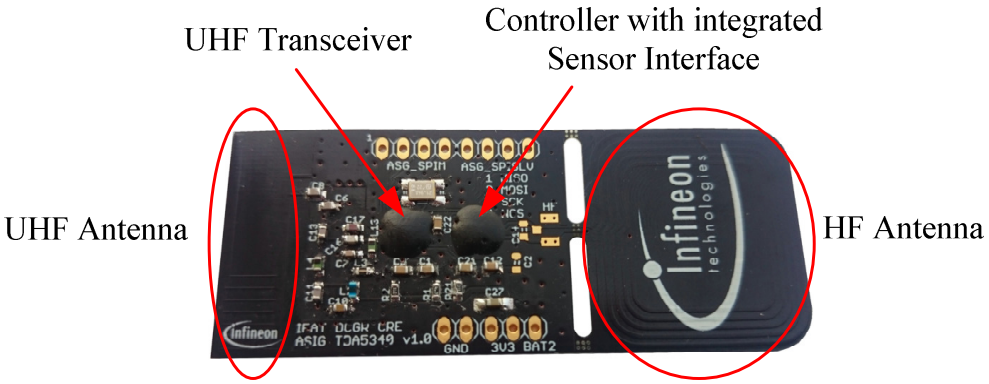

Figure 6.5: The manufactured wireless sensor node on the PCB

In Figure 6.5 the manufactured wireless sensor node is presented.

6.3 Firmware

A test firmware was written to verify the functionality of the produced sensor node. To achieve this, existing software for the controller chip (ASIG) was analyzed and modified. It turned out, that the software for HF communication interface was fully functional. Therefore only the communication between the two chips as well as controlling software for the transceiver chip had to be realized. The functionality of the test firmware includes booting the transceiver chip, configuration and sending test packages (see Figure 6.6).

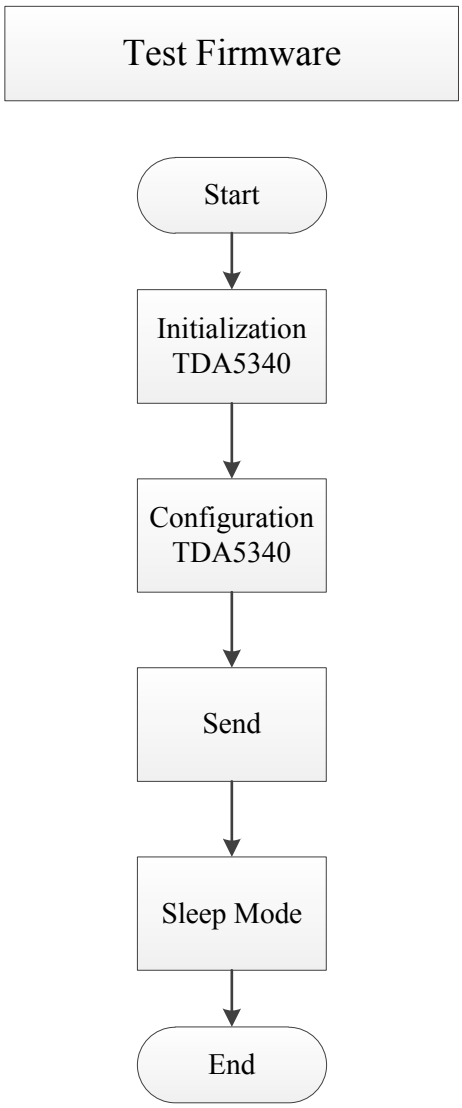

Figure 6.6: Blockdiagram of the developed test firmware

In Figure 6.7, a detailed view of the start up and configuration process is shown. Because this sequence is also processed when the TDA5340 is resuming from sleep mode, it is determined if the transceiver is already configured and ready to work. If this is not the case, the controller resets the power on pin of the transceiver and initializes a power on

reset (POR). After the POR is done successfully, the configuration of the transceiver is performed by the controller [12].

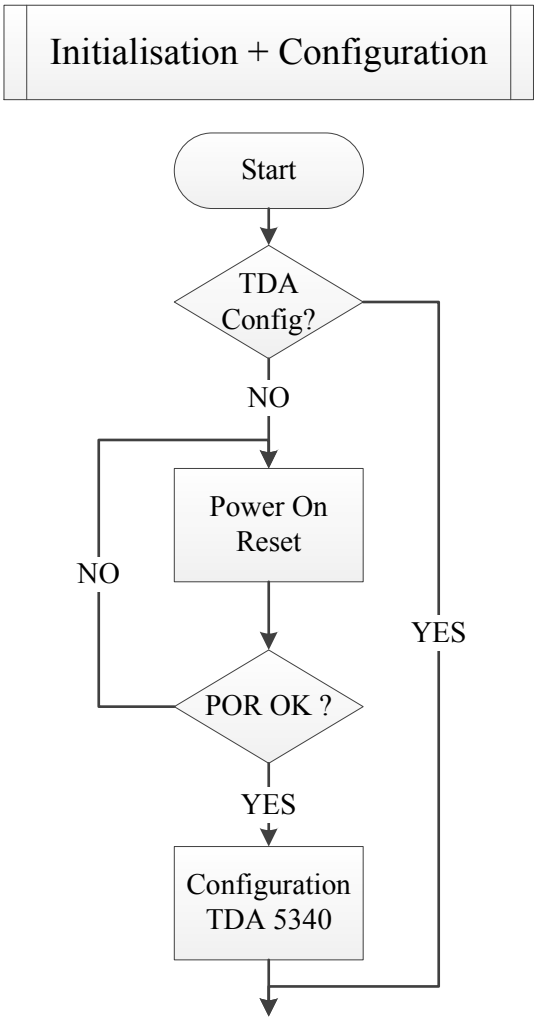

Figure 6.7: Blockdiagram: configuration of the TDA5340

The process for sending a test package is shown in Figure 6.8. First the controller sends the commands needed to switch the transceiver into send mode. To examine if this was done properly, the controller has to evaluate the data the transceivers interrupt status register. This read operation is necessary, because the controller does not provide interrupt inputs, and, therefore, it is not able to receive interrupt requests (IRQ) of the transceiver. If the transceiver successfully entered the send mode, the transceiver is now ready to transmit data using his UHF interface. The data has to be provided by the controller and written into the transmit-FIFO of the transceiver, including the information of data quantity. As soon as data is written into the FIFO, the transceiver starts transmitting until the FIFO is empty. After the transmission is completed, the transceiver enters sleep mode again.

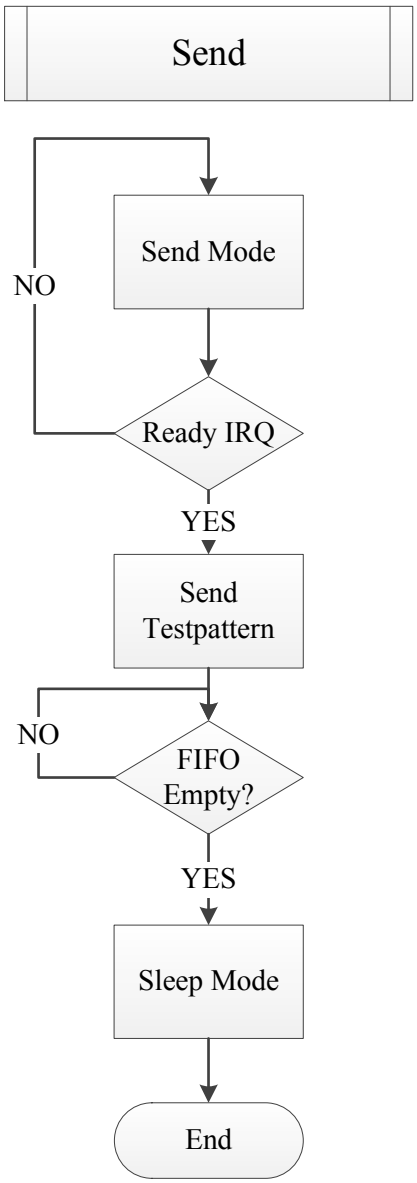

Figure 6.8: Blockdiagram: send test pattern

Chapter 7

Antenna Measurements

In the following chapter the performance of the manufactured PCB antennas was analyzed. To determine the performance of the antennas under real working conditions, it was decided to perform the measurement in a laboratory instead of a measuring chamber. The measurements are limited to the investigation of the reflection coefficient of the antennas to primarily find out, if the matching of the antennas meets the simulation results. The measurements were done using a network vector analyzer (VNA). The measurement setup can be seen in Figure 7.1; the device under test was put onto a wooden table and connected to the network analyzer using a 50 Ω transmission line. Before performing the measurement, the VNA was calibrated using a SOL (short-open-load) calibration kit at the end of the transmission line. This is required to define the reference plane and reference impedance for the VNA.

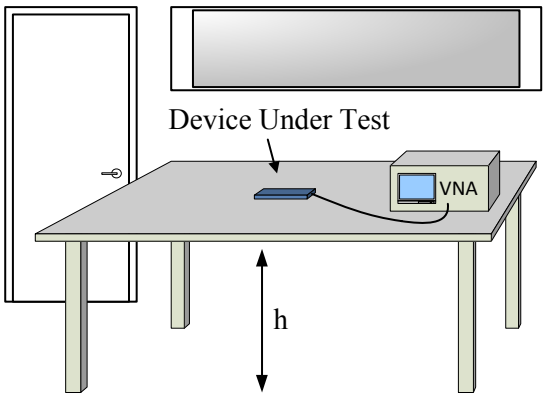

Figure 7.1: Measurement setup used for investigating the reflection coefficient of the different antennas

The primary goal of the antenna measurements was on determining the reflection coefficient and antenna impedance at the required frequency of 868 MHz and the development

of a matching network if needed.

7.1 Inverted F Antennas

IFAv1

The inverted F antennas where chosen because of their property to avoid any additional matching network. But as mentioned in Chapter 5, the precondition for achieving this is a very exact simulation of the antenna. Because the measurements were carried out under real circumstances, some deviations of the measurements compared to the simulation were expected. The results of the reflection coefficient measurement showed that the center frequency of the antenna IFAv1 was shifted from 869 MHz in the simulation to 917 MHz, and the reflection coefficient at this frequency was reduced to $\Gamma = -8\,\mathrm{dB}$. This shift also causes a performance loss at the targeted frequency of 868 MHz. Before continuing with the matching of the antenna to regain the desired performance needed for a proper functionality of the sensor node, some investigation is necessary to find out what happened. The possible reasons for this frequency shift and the subsequent performance loss can be:

- The permittivity of the dielectric substrate is different compared to the permittivity used in the simulation

- Influences during the measurement because of non ideal conditions

As mentioned in Chapter 2, the change of the permittivity of a dielectric substrate influences the propagation of electromagnetic waves. These influences are able to change the performance of the antenna. Figure 7.2 presents simulation results for the reflection coefficient of antenna IFAv1 for different permittivities of the FR4 substrate. The blue line shows the original simulation with $\epsilon = 4.6$ indicating the center frequency at 869 MHz. Reducing the permittivity of the substrate by 10 % causes a frequency shift of about 23 MHz upwards(green line). This is twice as much as the bandwidth of 11 MHz (see Section 5.2.1) provided by the antenna. Changing the permittivity by 20 % generates increases the center frequency of the antenna to 918 MHz. Hence, the narrow bandwidth of the antenna makes it vulnerable to fluctuations of the substrates permittivity.
The Smith Chart in Figure 7.3 shows the frequency response of the antenna impedance simulated with different substrate characteristics.

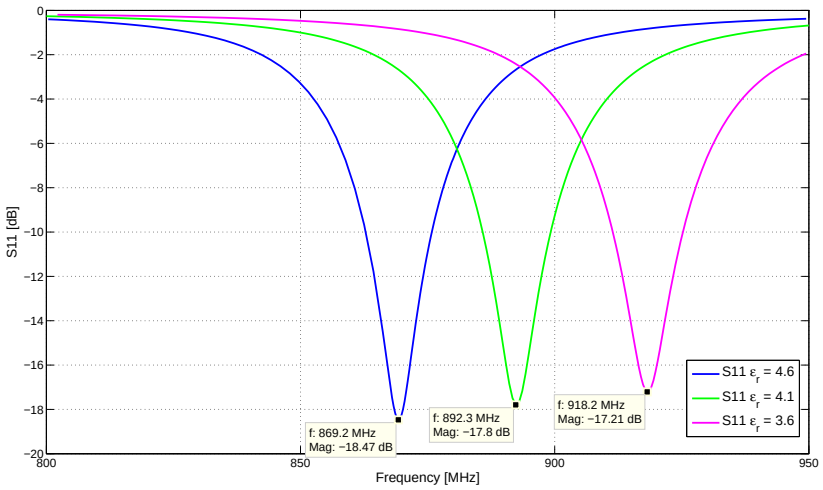

Figure 7.2: S11 simulation results of the IFAv1 antenna for different substrate permittivity

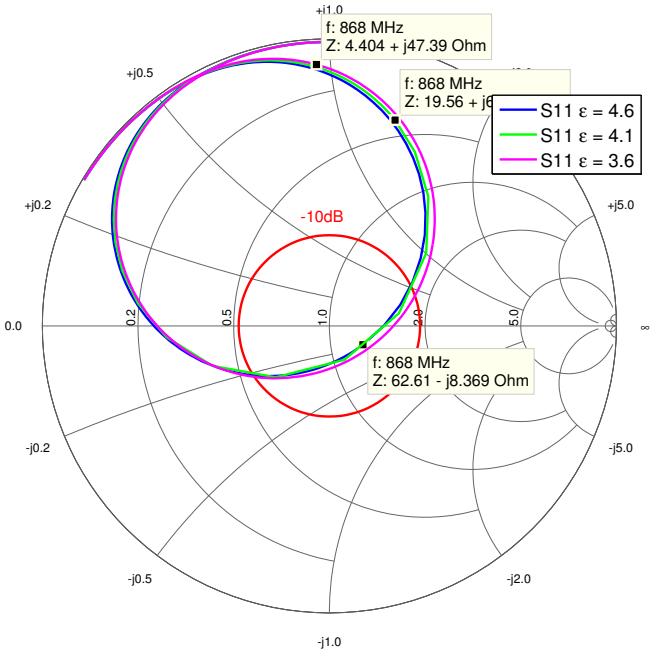

Figure 7.3: Simulation results of the IFAv1 antenna for different substrate permittivity plotted in the Smith Chart

In addition to the influences of changing permittivity, the quality of the measurement setup

and the surrounding environment has an impact on the measurement results. For example surface, where the device under test is lying on, also acts as substrate and changes the antenna characteristic. These investigations show that small effects can obviously change the performance of antenna.
Referring to the IFAv1, a matching network is necessary to achieve the needed reflection coefficient at the targeted frequency. In the Table 7.1 the measured antenna parameters are listed. The used matching network for the inverted F antennas is a L-network consisting of two capacitors; IFAv1: 8.2 pF in parallel and 5.6 pF in series, and IFAv2: 10 pF in parallel and 5.6 pF in series. The actual matching network was determined by iteratively changing the values of the L-network elements. The first approximation for the network elements was chosen with the help of the smith chart and improved by doing measurements again.

$f = 868\,\text{MHz}$		Impedance Z [Ω]	Reflection Coefficient S11 [dB]
IFAv1	unmatched	12+j74	-2
	matched	40.19-j5.1	-18.24
IFAv2	unmatched	2+j65	-2.5
	matched	44.12-j6.18	-20.87

Table 7.1: Measurement results for the inverted F antennas with and without additional matching at 868 MHz

The Figure 7.4 presents the measured reflection coefficient of IFAv1 with applied matching network. It can be seen that the antenna meets the target frequency of 868 MHz with sufficient accuracy. The bandwidth over which the reflection coefficient is below −10 dB, is about 15 MHz.

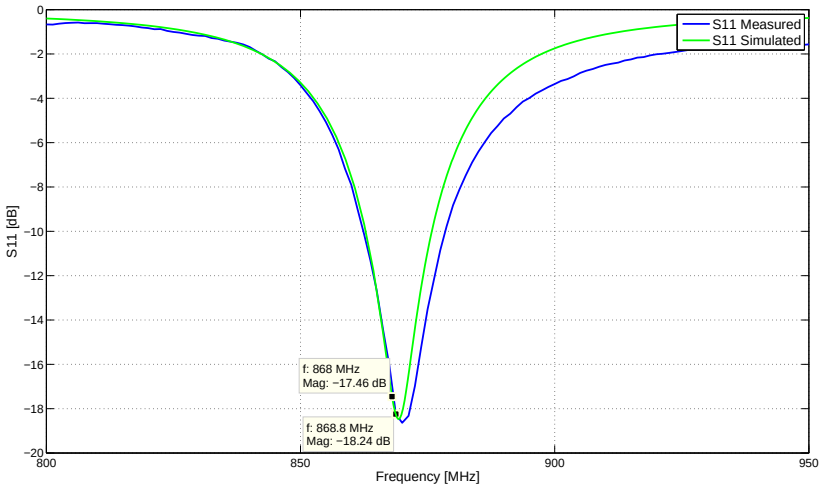

Figure 7.4: Results of the reflection coefficient measurement of antenna IFAv1 with applied matching network

The matched antenna is nearly resonant at 868 MHz as seen in the Smith Chart in Figure 7.5.

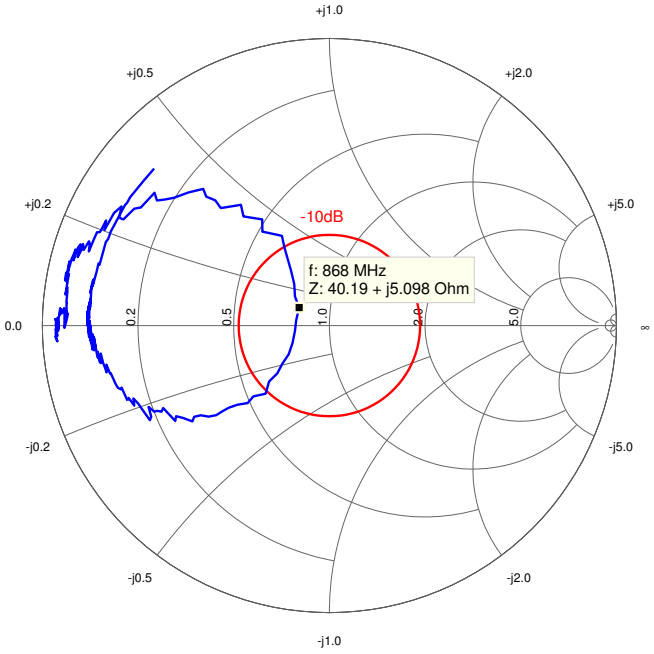

Figure 7.5: Smith diagram of antenna IFAv1

IFAv2

For the IFAv2, the effect is the same as mentioned above: the center frequency was shifted to 919 MHz. After applying the matching network the performance of antenna IFAv2 was increased and is characterized by Figure 7.6 and Figure 7.7. The matching for the IFAv2 is obviously better than for IFAv1. The bandwidth over which the reflection coefficient is below -10 dB, is about 20 MHz.

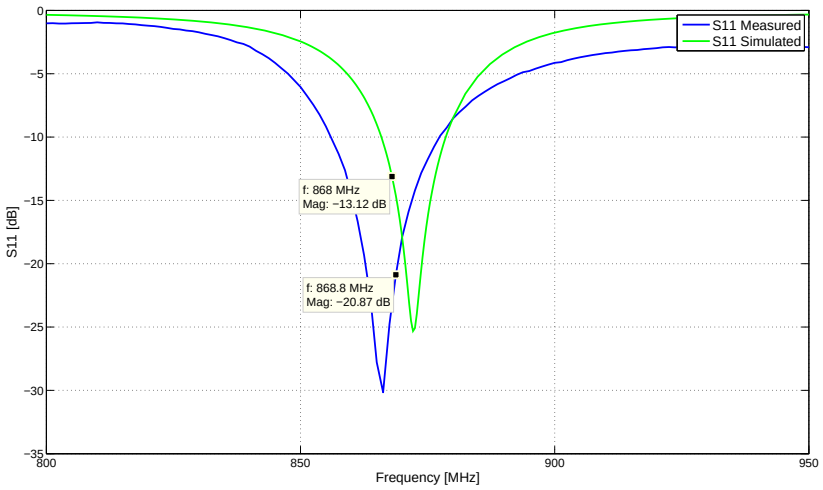

Figure 7.6: Results of the reflection coefficient measurement of antenna IFAv2 with applied matching network

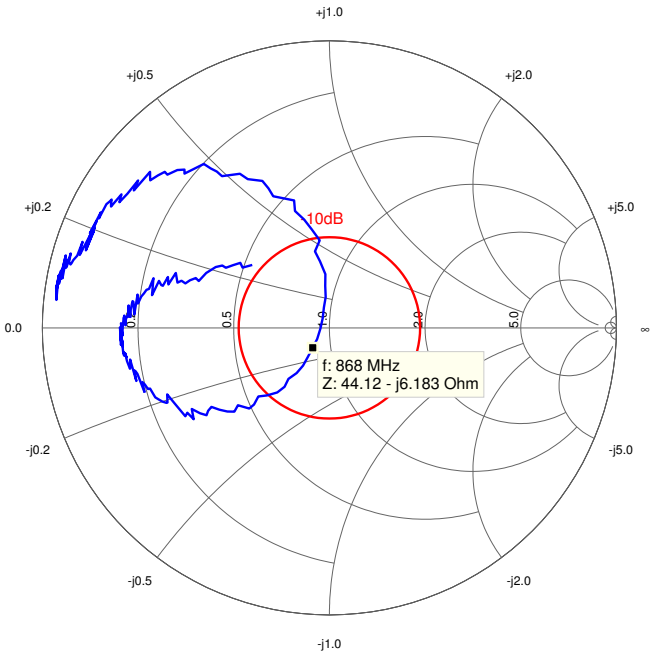

Figure 7.7: Smith diagram of antenna IFAv2

7.2 Loop Antenna

The measured performance of the loop antenna suffers under the same influences as mentioned inverted F antennas. The measured antenna impedance of the loop antenna is $Z = 18 + j62\,\Omega$ and the reflection coefficient equals $\Gamma = -2.4\,\text{dB}$. The matching network is also an L-network, consisting of two capacitors: 4.7 pF in parallel and 10 pF in series. In Figure 7.8 the reflection coefficient at the target frequency of the antenna $\Gamma = -15.91\,\text{dB}$ is indicated. The bandwidth at the center frequency of 871 MHz over which the reflection coefficient is below $-10\,\text{dB}$, is about 11.25 MHz.

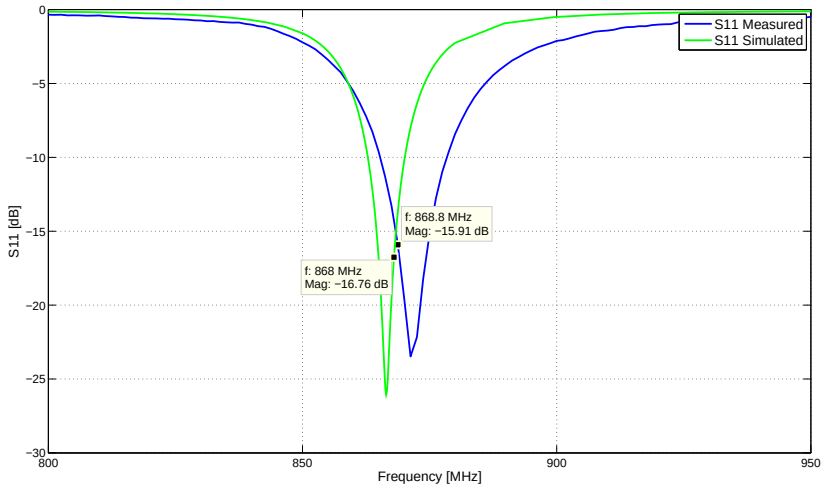

Figure 7.8: Results of the reflection coefficient measurement of the loop antenna with applied matching network

Figure 7.9 depicts the measured antenna impedance in the Smith Chart.

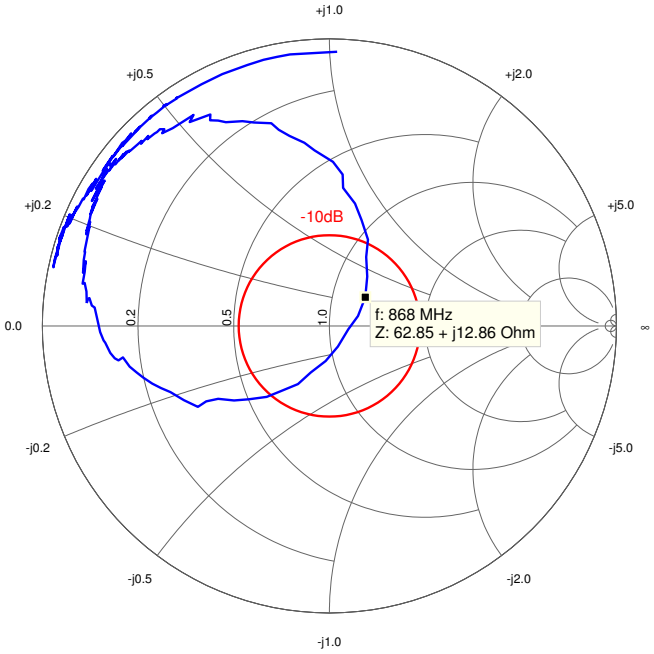

Figure 7.9: Smith diagram of the loop antenna

7.3 Monopole Antenna

The monopole antenna shows better consistency of the simulation and measurement results than the previously described ones. The design of this antenna supposed an additional matching network by default. That is why the measured unmatched antenna impedance of $Z = 10 - j42\,\Omega$ lies in the range, expected from simulation. The reflection coefficient in this case equals $\Gamma = -2.2\,\text{dB}$. As in the previous cases, the matching network is an L-network; but as this antenna is highly capacitive, the matching network consists of two inductors: 3.9 nH in parallel and 8.7 nH in series.

As it can be seen from the Figure 7.10, the antenna is sufficiently matched. The measured reflection coefficient of the antenna with applied matching network is $\Gamma = -20.9\,\text{dB}$. The bandwidth over which the reflection coefficient is below $-10\,\text{dB}$, is about 30 MHz at a center frequency of 872 [MHz.

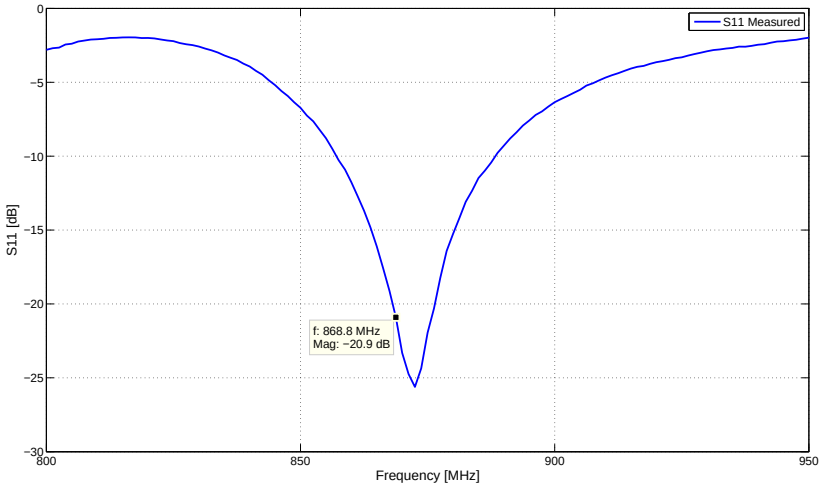

Figure 7.10: Results of the reflection coefficient measurement of the monopole antenna with applied matching network

The Smith Chart depicting the measured monopole antenna impedance is shown Figure 7.11.

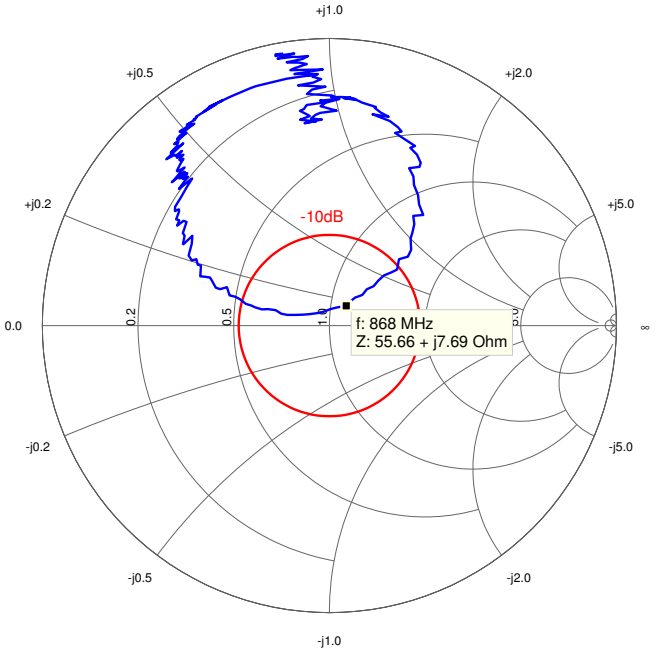

Figure 7.11: Smith diagram of the monopole antenna

Chapter 8

Conclusion and Outlook

In this thesis, a wireless sensor node, focusing on the HF and UHF communication interfaces, was designed. Two approaches were implemented: a highly miniaturized System in Package design (eWLB) and an implementation on a printed circuit board. The electric circuit of the node was designed, mainly consisting of a microcontroller and a transceiver chip, connected to an UHF antenna via a matching network. To evaluate different approaches, multiple UHF antennas for these implementations were designed and analyzed.

eWLB Design

The advantage of the eWLB design is the high miniaturization potential of this technology. At the same time, reduced size for antennas always results in a lack of performance. Hence, the designed antennas suffer from the small antenna area and the practically not existing ground plane on the eWLB. This interrelationship was verified by simulation results. However, the eWLB implementation was not manufactured yet, and the real performance of these antennas is still an open question.

Implementation on a Printed Circuit Board

The implementation of the printed circuit board was accomplished and a firmware was written for testing. All basic functions of the produced sensor node were working properly. Multiple different antennas for the UHF interface were designed, simulated and analyzed. The simulation results showed that the small ground plane and electric losses have a great impact on the antennas radiation efficiency. The evaluation of the manufactured antennas demonstrated differences in comparison to the simulation results. It turned out, the permittivity of the dielectric substrate of the PCB is different to the supposed value. Hence, the PCB with FR4 substrate is not the best solution for this application. These effects have minor influence on the monopole antenna, because it was unmatched anyway. After applying a proper matching network, the monopole antenna shows the best performance of all designed antennas.

Outlook

To increase the performance of the antennas, there are multiple options for further enhancements. First of all, to overcome the problems according to the imprecise permittivity, a different substrate with a more homogeneous substrate with definite permittivity; this however, leads to increased cost of the system. An alternative would be use of a tunable matching network to compensate the effect of the different permittivity. Furthermore, some improvements on the PCB layout level can be done: avoid connections on the bottom layer to introduce a uniform ground plane; these improvements definitely have positive influences on the antennas radiation performance. Additionally, there is a possibility to extend the firmware with perspective of customized product development. The extension of the firmware should include all software modules enabling communication with the control unit in normal operation mode, as explained in Chapter 4.

Appendix A

Schematics and Layout documents

This section provides a collection of electrical schematics and layout documents of the wireless sensor node.

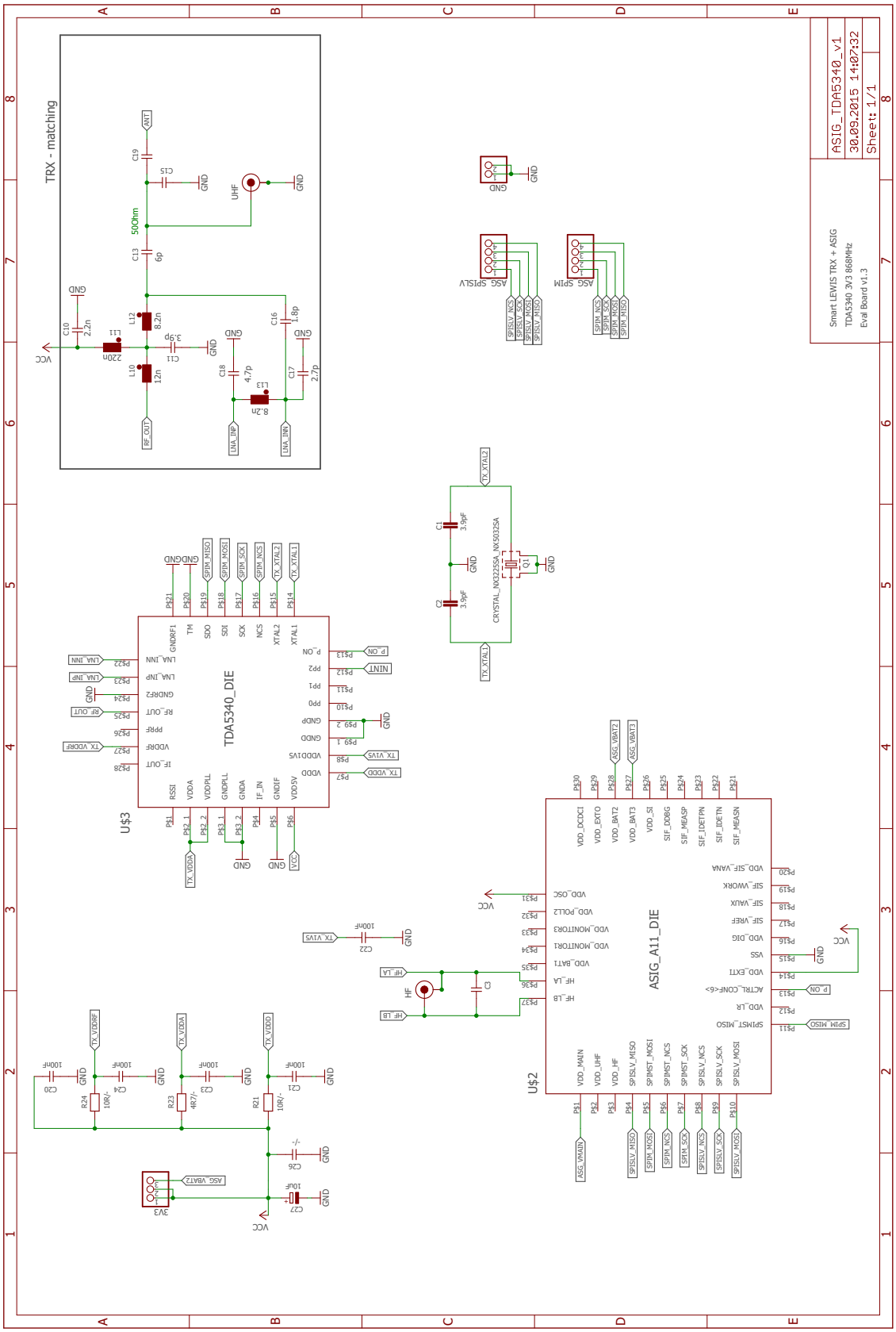

Figure A.1: Schematic of the wireless sensor node

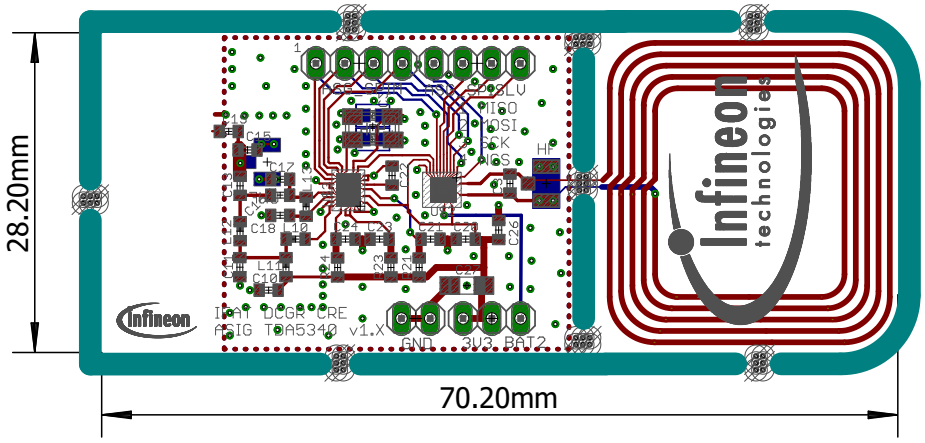

Figure A.2: Layout of the wireless sensor node

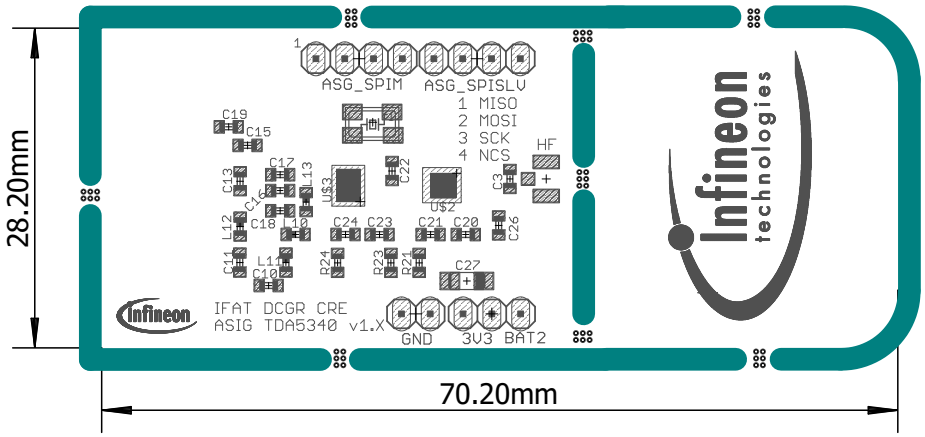

Figure A.3: Layout of placement TOP side

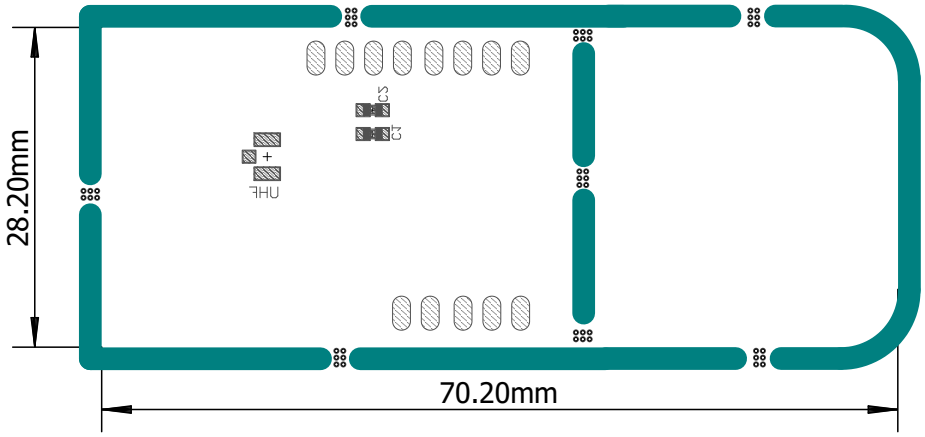

Figure A.4: Layout of placement BOTTOM side

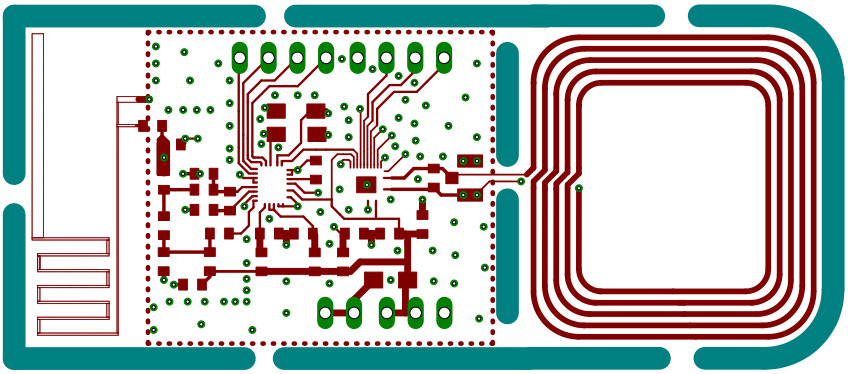

Figure A.5: TOP layer

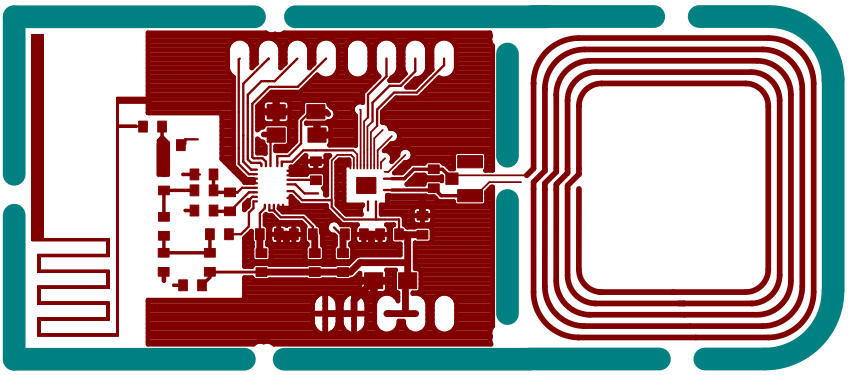

Figure A.6: Layout of metal layer TOP side with IFav1

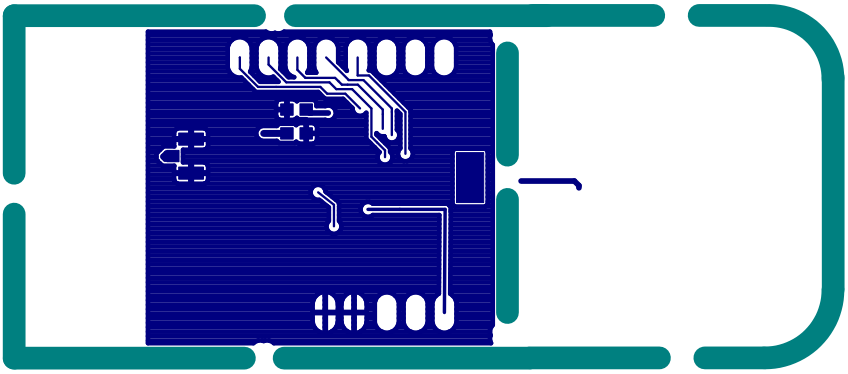

Figure A.7: Layout of metal layer BOTTOM side

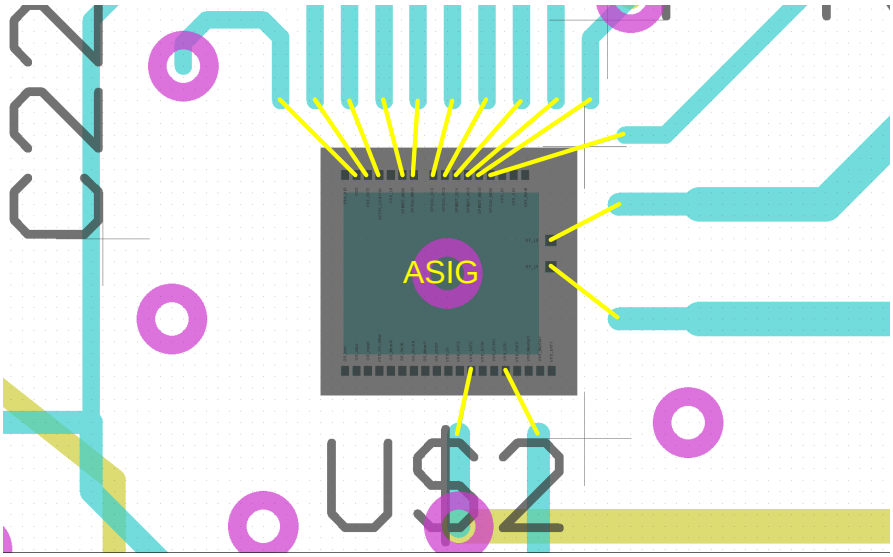

Figure A.8: Bonding plan for the ASIG controller

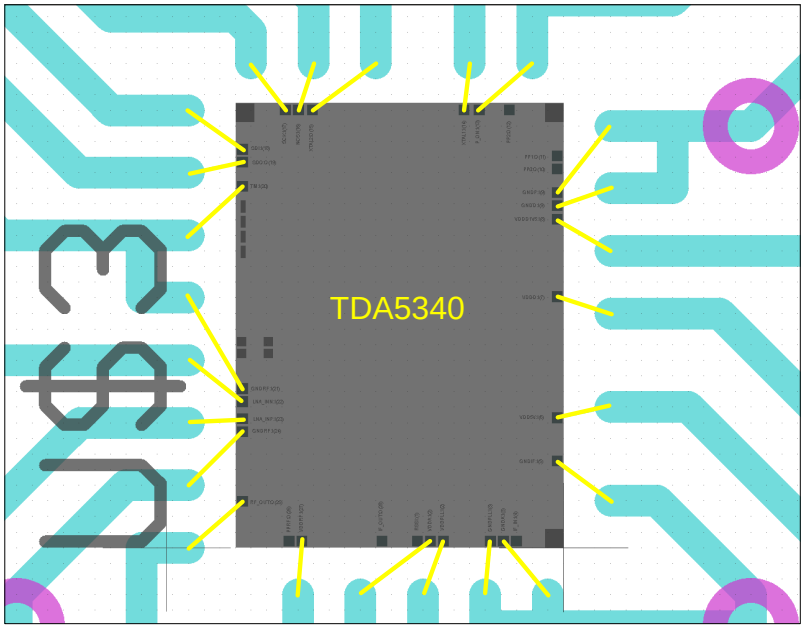

Figure A.9: Bonding plan for the transceiver TDA5340 controller

Bibliography

[1] W. L. Stutzman and G. A. Thiele, *Antenna Theory and Design*, 3rd ed. Wiley, 2012.

[2] T.Meyer, K.Pressel, G.Ofner, and B.Römer, "System integration with ewlb," in *Electronic System-Integration Technology Conference (ESTC), 2010 3rd*, 2010.

[3] W. Pachler, K. Pressel, J. Grosinger, G. Beer, W. Bösch, G. Holweg, C. Zilch, and M. Meindl, "A novel 3d packaging concept for rf powered sensor grains," in *ECTC 2014*, 2014.

[4] C. A. Balanis, *Modern Antenna Handbook*. Wiley, 2008.

[5] D. M. Pozar, *Microwave Engineering*, 4th ed. Wiley, 2012.

[6] H. Heuermann, *Hochfrequenztechnik*, 2nd ed. Vieweg, 2009.

[7] D.G.Fang, *Antenna Theory and Microstrip Antennas*. CRC Press, 2010.

[8] K. Fujimoto, Ed., *Mobile Antenna System Handbook*, 3rd ed. Artech House, 2008.

[9] G. Marrocco, "The art of uhf rfid antenna design: Impedance-matching and size-reduction techniques," *IEEE Antennas and Propagation Magazine*, vol. 50, no. 1, pp. 66–79, 2 2008.

[10] M. PourMousavi, M.Wojonowski, R. Agethen, and A.-H. R-Weigel, "The impact of embedded wafer level bga package on the antenna performance," in *Antennas and Propagation in Wireless Communications (APWC), 2013 IEEE-APS Topical Conference on*, 2013.

[11] A. Jonjic, J. Grosinger, T. Herndl, R. Matischek, G. Holweg, and W. Boesch, "A secruity and nfc enhanced wireless sensor network node," in *in Proc. IEEE Sensors, Valencia*, 2014.

[12] "Tda 5340 high sensitivity multi-channel transceiver user manual v1.0," 2 2012.

[13] "Tda 5340 high sensitivity multi-channel transceiver datasheet v1.2," 6 2012.

[14] "Tda 5340 protocol examples for ism band applications," 2012.

[15] T. G. Company, "Material datasheet: Nema grade fr4 glass epoxy laminate."

[16] V. Europe, “Material datasheet: Vt-481 fr4.”

[17] www.aetzwerk.de, “Homepage of www.aetzwerk.de, manufacturer of printed circuit boards.”